NUREG/CR-5422

Performance of the Liquid Reactivity Control System in BWRs

Prepared by T. G. Theofanous, E. A. Shabana

Department of Chemical and Nuclear Engineering
University of California

Prepared for
U.S. Nuclear Regulatory Commission

AVAILABILITY NOTICE

Availability of Reference Materials Cited in NRC Publications

Most documents cited in NRC publications will be available from one of the following sources:

1. The NRC Public Document Room, 2120 L Street, NW, Lower Level, Washington, DC 20555
2. The Superintendent of Documents, U.S. Government Printing Office, P.O. Box 37082, Washington, DC 20013-7082
3. The National Technical Information Service, Springfield, VA 22161

Although the listing that follows represents the majority of documents cited in NRC publications, it is not intended to be exhaustive.

Referenced documents available for inspection and copying for a fee from the NRC Public Document Room include NRC correspondence and internal NRC memoranda; NRC Office of Inspection and Enforcement bulletins, circulars, information notices, inspection and investigation notices; Licensee Event Reports; vendor reports and correspondence; Commission papers; and applicant and licensee documents and correspondence.

The following documents in the NUREG series are available for purchase from the GPO Sales Program: formal NRC staff and contractor reports, NRC-sponsored conference proceedings, and NRC booklets and brochures. Also available are Regulatory Guides, NRC regulations in the *Code of Federal Regulations*, and *Nuclear Regulatory Commission Issuances*.

Documents available from the National Technical Information Service include NUREG series reports and technical reports prepared by other federal agencies and reports prepared by the Atomic Energy Commission, forerunner agency to the Nuclear Regulatory Commission.

Documents available from public and special technical libraries include all open literature items, such as books, journal and periodical articles, and transactions. *Federal Register* notices, federal and state legislation, and congressional reports can usually be obtained from these libraries.

Documents such as theses, dissertations, foreign reports and translations, and non-NRC conference proceedings are available for purchase from the organization sponsoring the publication cited.

Single copies of NRC draft reports are available free, to the extent of supply, upon written request to the Office of Information Resources Management, Distribution Section, U.S. Nuclear Regulatory Commission, Washington, DC 20555.

Copies of industry codes and standards used in a substantive manner in the NRC regulatory process are maintained at the NRC Library, 7920 Norfolk Avenue, Bethesda, Maryland, and are available there for reference use by the public. Codes and standards are usually copyrighted and may be purchased from the originating organization or, if they are American National Standards, from the American National Standards Institute, 1430 Broadway, New York, NY 10018.

DISCLAIMER NOTICE

NUREG/CR-5422
R4

Performance of the Liquid Reactivity Control System in BWRs

Manuscript Completed: January 1989
Date Published: September 1989

Prepared by
T. G. Theofanous, E. A. Shabana

Department of Chemical and Nuclear Engineering
University of California
Santa Barbara, CA 93106

Prepared for
Division of Regulatory Applications
Office of Nuclear Regulatory Research
U.S. Nuclear Regulatory Commission
Washington, DC 20555
NRC FIN D1634

ABSTRACT

Boiling water reactors rely on the injection of soluble neutron absorbers to control power in case of failure in the control rod (scram) system. Typically this liquid "poison" is injected from eight small holes on a standpipe positioned vertically near the outer edge of the core shroud in the lower plenum. The achievement of control is predicated on good mixing of this injected liquid with the coolant which is recirculating around the core upper plenum and downcomer. However, because the flows are rather low (~20% of rated with pumps tripped as expected under such conditions) and the injected solution density is much higher than that of the primary fluid, there have been concerns raised about the efficiency and completeness of this mixing. This work provides the first openly available data addressing such concerns. To avoid potentially important scaling compromises, the data were obtained from full-scale simulations. From the experiments performed so far, we can conclude that complete boron mixing (entrainment) will occur for recirculation flow rates down to 8.2% of rated.

TABLE OF CONTENTS

LIST OF FIGURES

LIST OF FIGURES — CONT.

LIST OF TABLES

ACKNOWLEDGMENTS

This work was performed for the U.S. Nuclear Regulatory Commission, under contract 0486-111. We are grateful to Mr. P. Hill (Pennsylvania Power and Light Co.) for his interest in this work, his help with system information, and many insightful comments on the original manuscript.

1. INTRODUCTION

Many boiling water reactors (BWRs) rely on liquid poison (Standby Liquid Control System or SLCS), injected into the lower plenum, to achieve shutdown from postulated ATWS (anticipated transients without scram) events. Due to the combination of solute (sodium pentaborate) and temperature effects, the injection solution is ~35.5% heavier than the primary fluid, and the potential for its stratification into the lower plenum (settling rather than entering the core region, where it is needed) under the relatively low natural circulation flow velocities was recognized long ago. The General Electric (GE) Company has obtained mixing data in a 1/6-scale (geometric) simulation facility. These data remain proprietary, although the indications are that they exhibit a strong tendency to stratify for recirculation flows less than ~20% of rated. This is precisely the range of interest for the natural circulation flows relevant to postulated ATWS transients. This led to complicated operator procedures and an interest in modeling the mixing process in a form appropriate for use in system's codes (i.e., TRAC-BWR).

The complications arising from inadequate mixing can be understood in terms of Figure 1, obtained from a 1982 BWR Owner's Group letter to the Nuclear Regulatory Commission (NRC) (BWR Owner's[1]). In it, mixing efficiency is seen to approach zero at ~5% of rated flow, while it seems to reach a nearly constant upper value of ~75% for flows higher than 20% of rated. On the other hand, the core power shows a linear decrease with recirculation flow, due to corresponding increases in core void (steam) fraction. The combined effect on an ATWS transient is to produce the strongly upward concave curve of suppression pool temperature, as shown in Figure 1. That is, at high flows the suppression pool overheats as the boron mixing cannot keep up with the steam production. At very low flows, on the other hand, the whole transient is prolonged such that suppression pool overheating is obtained even at the low power levels.

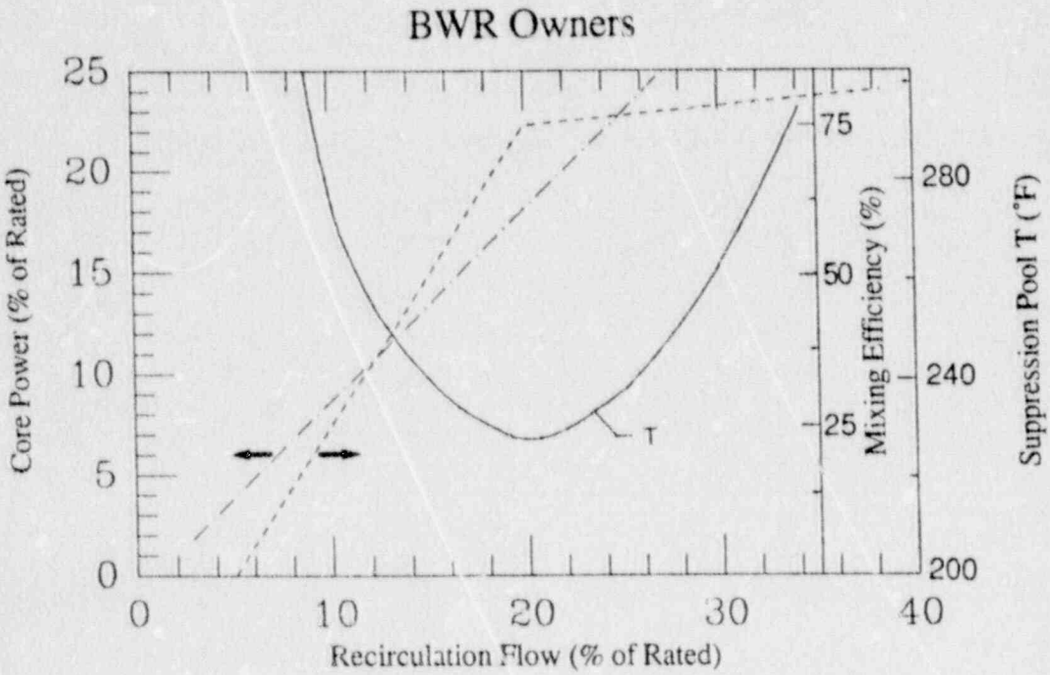

Fig. 1. *Boron mixing efficiency, associated power, and suppression pool overheating as a function of recirculation [1].*

Additional perspectives on the behavior can be obtained from Figures 2 and 3, reproduced from Chexal et al.[2], who ignored the SLCS altogether. The critical path in Figure 2 shows the decrease in core power and associated decrease in recirculation (natural) flow resulting from dropping the water level from the normal downcomer water level (NWL) to the top of active fuel (TAF) at normal operating pressure. The critical path in Figure 3 indicates the effect of depressurization on the same variables. It is clear from these figures that power reduction to sufficiently low levels can come about only by a combined and *decisive* reduction in both water and pressure levels. It is also clear that the relevant recirculation flows are in the range 10 to 30% of rated. Finally, in subjecting the plant to these low-power, low-flow conditions, one needs to be concerned about the potential occurrence and impact of coupled flow-power instabilities, as recently manifested in the La Salle incident.

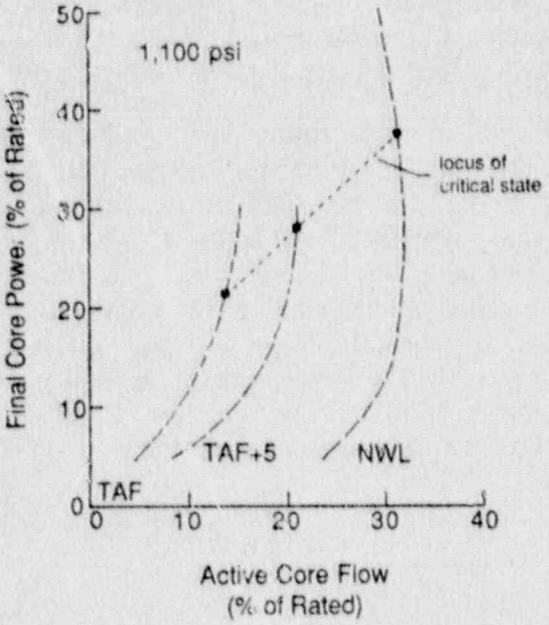

Fig. 2. *Final core power versus active core flow at various downcomer levels [2].*

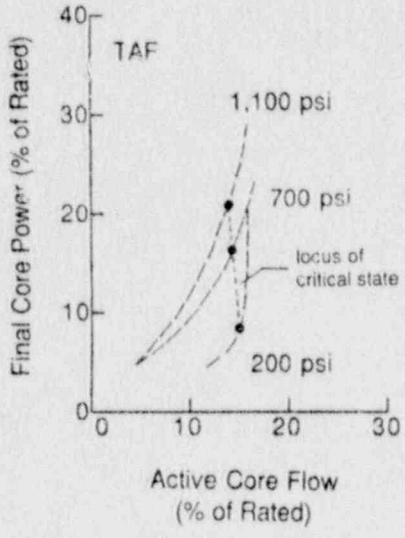

Fig. 3. *Final core power versus total core flow at various system pressures [2].*

Based on the above as an initial ATWS fix, the operators were instructed to reduce water levels to the top of the active core. More recently, as an update to this procedure, there is a proposal in front of the NRC-licensing that the water level be dropped below the top of the active core in order to achieve an acceptable performance under such conditions. Clearly, such procedures are not particularly attractive if they can be avoided. These then provide a motivation for a closer examination of the boron mixing phenomena, which is the subject of this study.

In this report we provide a new experimental approach. The initial experimental data indicate considerable promise that mixing is complete and that the special procedures discussed above may not be necessary.

2. SCALING CONSIDERATIONS

The lower plenum geometry of interest is shown in Figure 4. The actual positioning of the injection line (SLCS standpipe) within the control rod guide array is indicated for two representative designs (BWR3s and BWR4s) in Figure 5. The key dimensions and characteristics are summarized in Table 1, below:

TABLE 1

Geometric Features of SLCS

Plant	A[1]	B[2]	C[3]	Pipe Size	# of Holes[4]	Hole Diameter
BWR3 (Dresden 3)	2.6"	42"	9.4"	1" SCH40	8	0.25"
BWR4 (Peach Bottom 3)	6.1"	42"	14.8"	1" SCH40	8	0.25"

Note: All dimensions in inches, holes directed towards vessel center.
1 distance from the centerline of the SLCS standpipe to the shroud inside diameter.
2 length over which sparger holes are spaced.
3 distance of the lowest hole above the shroud support plate.
4 equally spaced along the standpipe at 3" intervals.

Typical injection rates are 60 to 80 gpm of borated water (15% by weight sodium pentaborate in 20 °C water). We are interested in determining the fraction of this injected flow that enters the core region, entrained by the buoyancy-driven recirculating coolant flow.

We can identify two mixing regimes. The first, or vertical (upward) mixing regime (VMR), is obtained as the mean flow streams along the control rod guide tubes while the injected solution jets in a direction cross to it, as illustrated (for one hole) in Figure 6. This figure also shows the entrainment patterns created by the intense jet effect. The second, or horizontal mixing regime (HMR), may be obtained in case some solution settles downward, having escaped entrainment from the VMR. It is characterized by the mean flow streaming across the guide tubes and the solution attempting to settle through it, as illustrated in Figure 7.

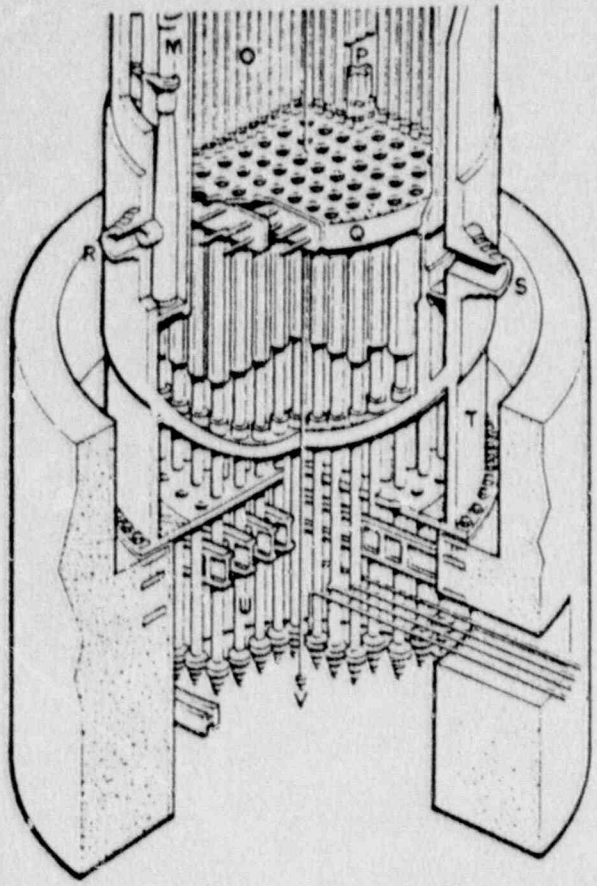

Fig. 4. *The lower plenum of a BWR.*

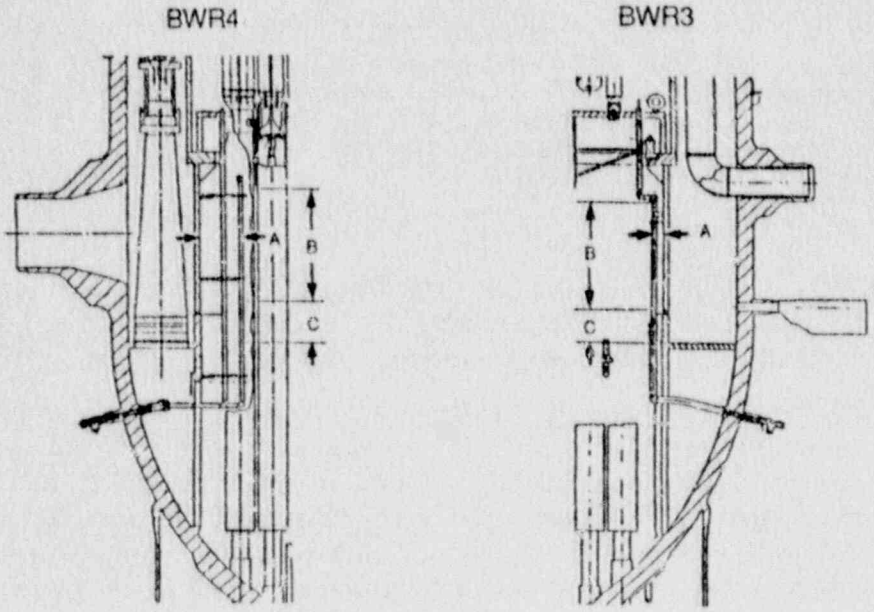

Fig. 5. *SLCS standpipe (injection) geometry.*

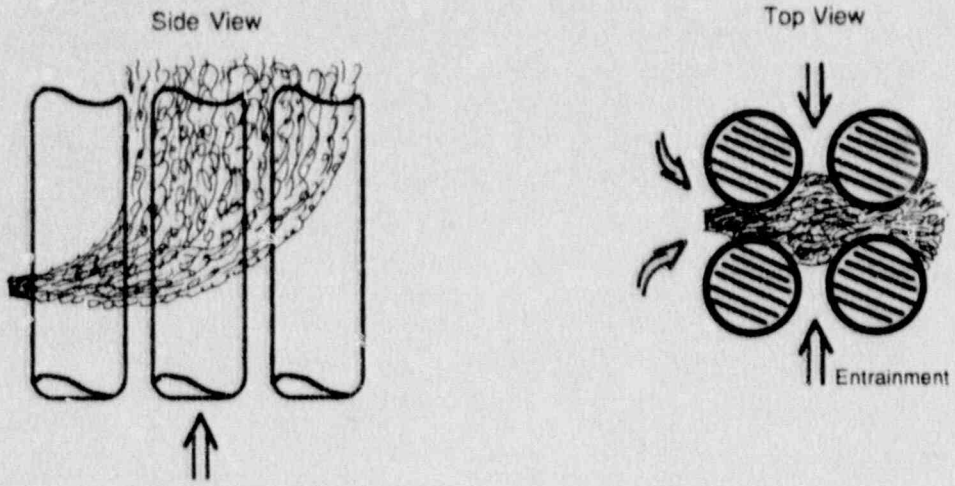

Fig. 6. *Illustration (not to scale) of the vertical mixing regime (VMR).*

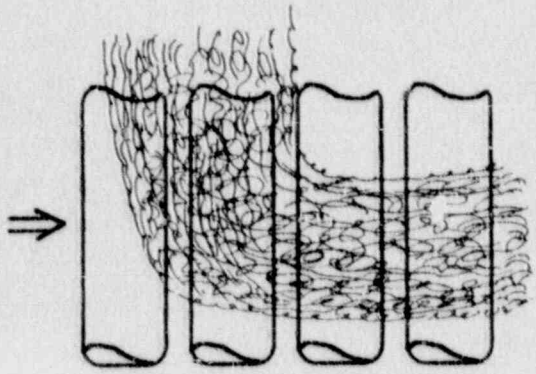

Fig. 7. *Illustration (not to scale) of the horizontal mixing regime (HMR).*

As it is customary for flows where gravitational effects are important, the GE experiments were scaled on the basis of the Froude number:

$$Fr = \frac{U}{\sqrt{gD\Delta\rho/\rho_I}}, \tag{1}$$

where U and D are the characteristic velocity and length scales, g is the acceleration of gravity, and $\Delta\rho = \rho_I - \rho_m$, where ρ_I and ρ_m are the densities of the injected and mean flow, respectively.

The problem is that at small scales such scaling can lead to very large Reynolds numbers dissimilarities. Indeed, as may be seen from Eq. 1, at 1/6-scale the characteristic velocity must be reduced by a factor of $\sqrt{6} \sim 2.5$, and the combined effect is a Reynolds number dissimilarity by a factor of $6 \times 2.5 \sim 15$. The scaling can further deteriorate due to inabilities to achieve the full $\Delta\rho/\rho_l$, and also because of the considerably larger kinematic viscosity in the experiment (low pressure and temperature system) in relation to the reactor. For example, the use of a

10% solution in the experiment would yield another factor of $\sim \sqrt{3.9}$ reduction in velocity, and together with the kinematic viscosity ($\sim$2) and scale effects, we will have a total factor of $\sim$59 dissimilarity in Reynolds number. All of these distortions are rather detrimental, especially when inertia and momentum flux effects are important, as is the case here due to the high injection Froude numbers and flow-penetrating-a-structure-array geometry.

Based on the above, it is not difficult to surmise that small scale simulations, in this area, may significantly underestimate mixing behavior. We decided, therefore, to pursue the problem at full scale.

3. EXPERIMENTAL FACILITIES

3.1 Vertical Mixing Regime

The UCSB VMR full-scale facility is shown in perspective in Figure 8. It represents a 3x3 array of control rod guide tubes in the vicinity of the SLCS standpipe. Axial flow is provided by a centrifugal pump, at up to 2,300 gpm (corresponding to 32% of rated), through a 2,000 gal recirculation stainless-steel tank, and it is controlled by a butterfly valve. The flow is distributed by means of deflector vanes, in the lower plenum, and straightened by honeycomb plates, prior to entering the subchannel space of the test section, and also as it exits into the outlet plenum. The UCSB VMR full-scale test section, shown in Figure 9, is accessible to full visualization---both guide tubes and pressure boundary are acrylic. All piping external to the test section is of PVC material. Injection flow is provided by a positive displacement pump (at full reactor flows, i.e., $\sim$10 gpm per nozzle) from a 200-gal. storage tank into any number of the injection nozzles (corresponding to the SLCS standpipe holes) by opening the appropriate ball valves (Figure 10(c)). The recirculating flow is measured by a nozzle insert and the injected flow by an orifice meter, both calibrated to an accuracy of $\pm$2%.

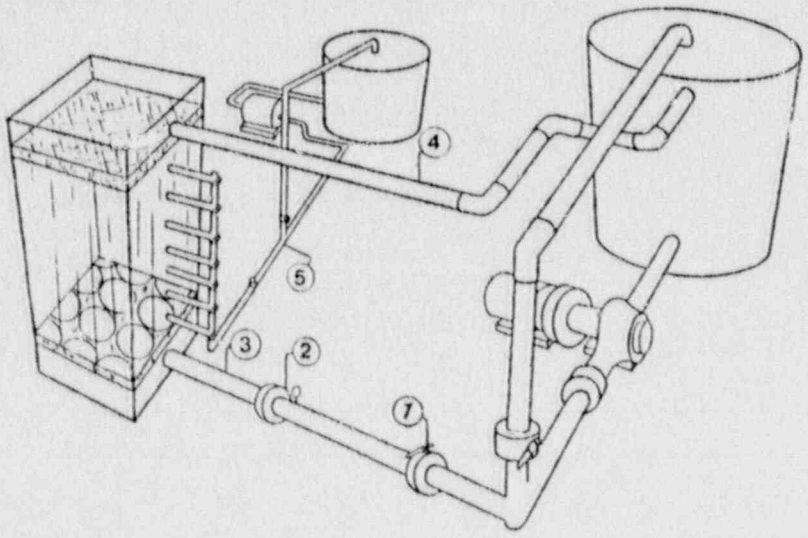

Fig. 8. *The UCSB VMR full-scale facility.*
(1) flow butterfly valve; (2) flow measuring nozzle;
(3) inlet probe; (4) outlet probe; (5) injection system.

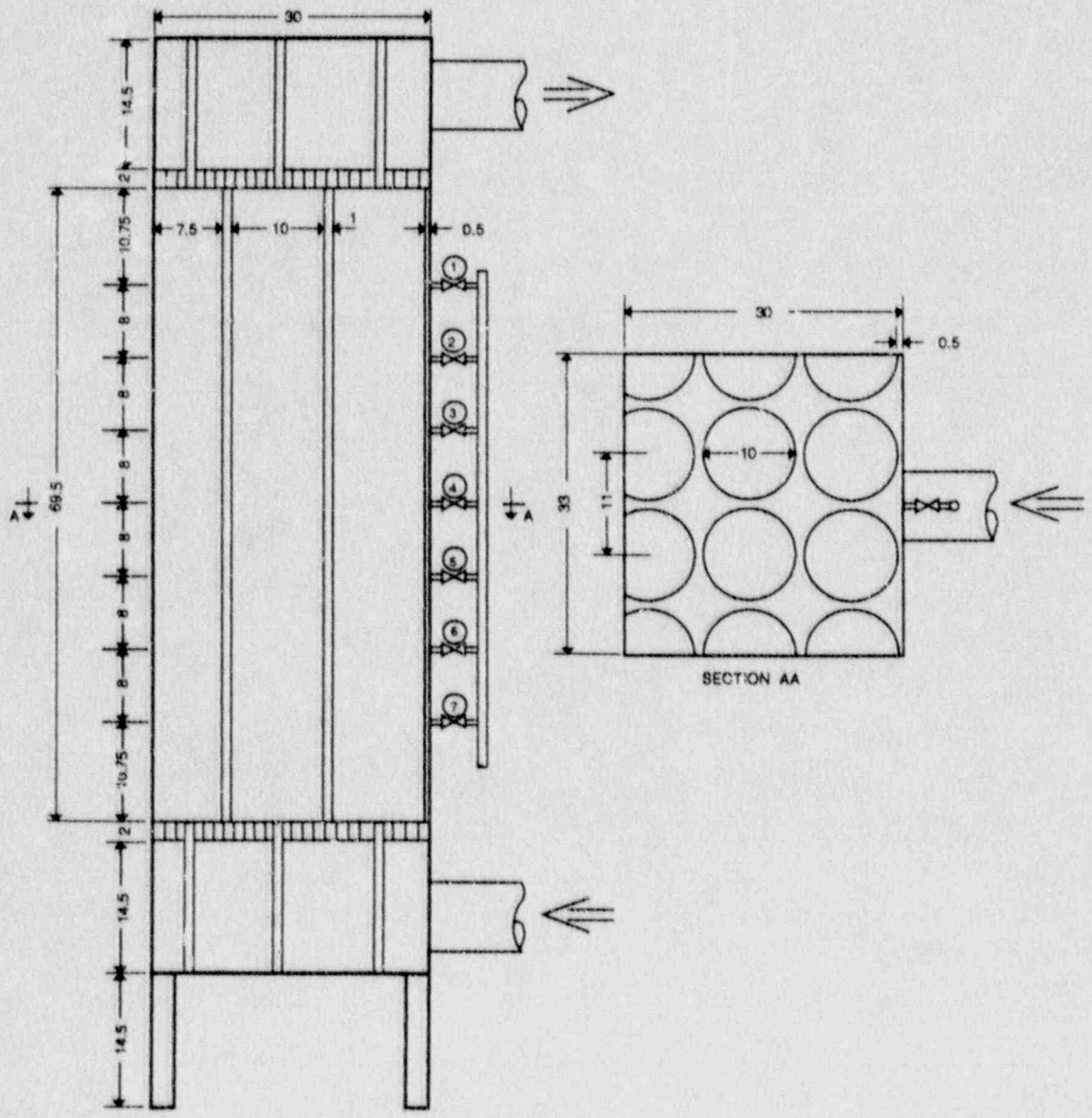

Fig. 9. *The UCSB VMR full-scale test section.* (All dimensions in inches.)

The solutions are made with $CaC\ell_2$ (up to 40% by weight); concentrations in the test section and inlet/outlet piping can be measured by conductivity probes (Theofanous et al.[3]). Overall mixing performance can be determined from the difference between inlet and exit concentrations and appropriate mass balances. Local mixing performance can be determined from a large number of conductivity probes distributed throughout the subchannel space in the test section. The data are taken by a PDP-11 computer at a rate of 500 Hz and recorded at a rate of 5 Hz (averaged over time increments of 1 s for each probe) and subsequently analyzed on the University VAX computer. Frequent calibration of the probes indicated high-reliability measurements with an accuracy of $\pm 2\%$ of the full-range density difference 0.025 g/cm^3.

Visualization data are also obtained by coloring the injection tank contents and using a video system. A secondary injection system (not shown) can provide short pulses of solution into the bottom of each subchannel to visualize and measure (from the time to traverse two axial probe positions) respective subchannel velocities. A two-velocity fiber optic LDA is also available for local velocity measurements at latter stages of this study.

Pictorials of the overall experimental arrangement, the test section, and the injection system are shown in Figure 10 (a-c).

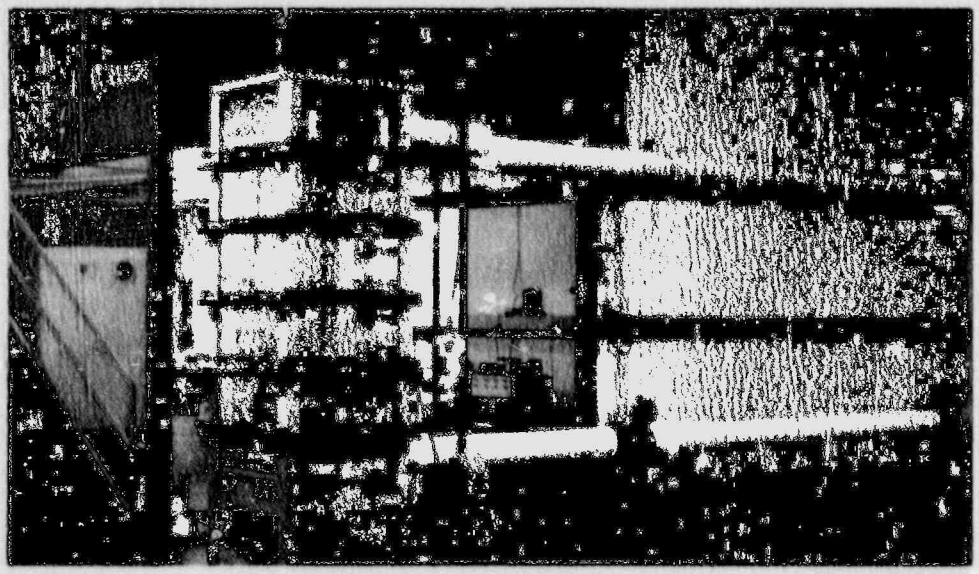

Fig. 10a. *Overall experimental setup.*

3.2 Horizontal Mixing Regime

Here we make use of an existing flume in the adjacent Ocean Engineering Laboratory (Figure 11) fitted by the 3x3 square grid array of control tube guides. The flume can provide up to 5,500 gpm over a flow cross section of 37.75 × 35.25 inch (tube height, outside diameter and center to center distance are 37.75, 10.75, and 11.75 inches, respectively). Here the solution is distributed (rather than forcefully injected) at the top of the subchannel space of the first one or two rows, and the mixing behavior as it is convected across the tube array is followed by video recordings (conductivity probes are available for future measurements). Viability of this experimental arrangement has been demonstrated by scoping experiments; however, actual testing is scheduled to follow completion of the VMR series of runs (next year).

Fig. 10b. *Test section with conductivity probes in place.*

4. EXPERIMENTAL RESULTS AND DISCUSSION

In conjunction with development of the experimental techniques, an extensive set of experiments (visualizations) were run in both the VMR and the HMR facilities. Visualization data indicated a strong tendency toward complete mixing. Based on this initial information, the program was directed, accordingly, towards establishing the minimum boundaries for complete entrainment and mixing. An indication of the kind of data obtained at this stage is given in Figure 12 ($\rho_I = 1.4$ g/cm^3, 3-nozzle injection) and Figure 13.

In the second stage, we sought to identify such minimum boundaries for the VMR with a 3-nozzle injection. In this first stage of quantification we would have preferred to work with a single nozzle injection ($\sim$10 gpm); however, because of the large quantity of recirculating flow, from a measurement accuracy standpoint we felt more comfortable with a 3-nozzle, $\sim$30 gpm injection. Nozzles number 3, 4, and 5 counting from the top were utilized in these experiments. Three sets of experiments were performed with $CaC\ell_2$ ($\rho_I = 1.4$, 1.316, and 1.194 g/cm^3). In these sets, we exposed the injection solution to a variety of recirculating flows.

Typical data records (the test matrix containing the conditions of all runs can be found in Table A.1 in the appendix) for a significantly-stratified and a fully-entraining (100% mixing)

Fig. 10c. *The injection system.*

Fig. 11. *Flume utilized for studying the HMR.*

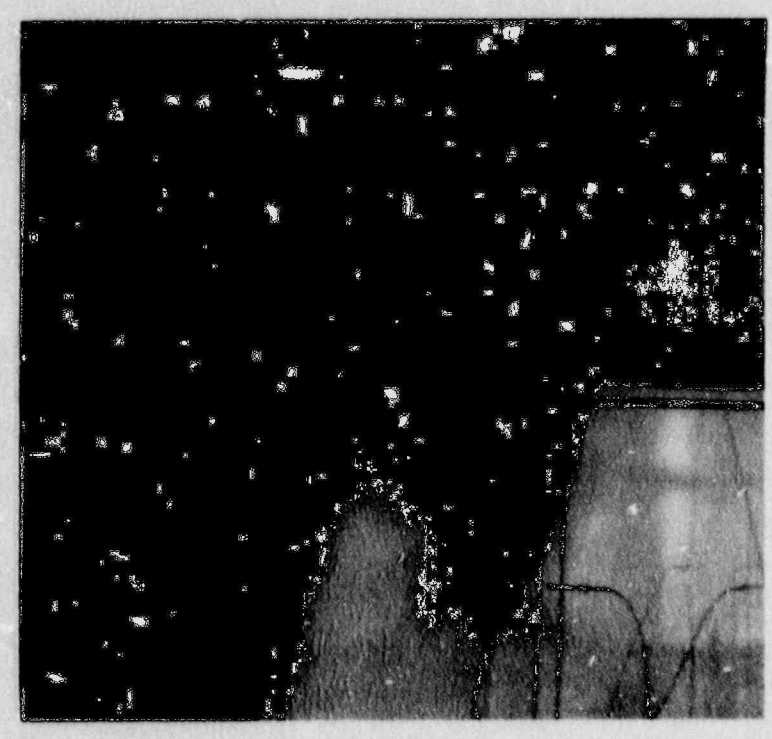

Fig. 12a. *The mixing phenomena in the VMR (full entrainment at 600 gpm).*

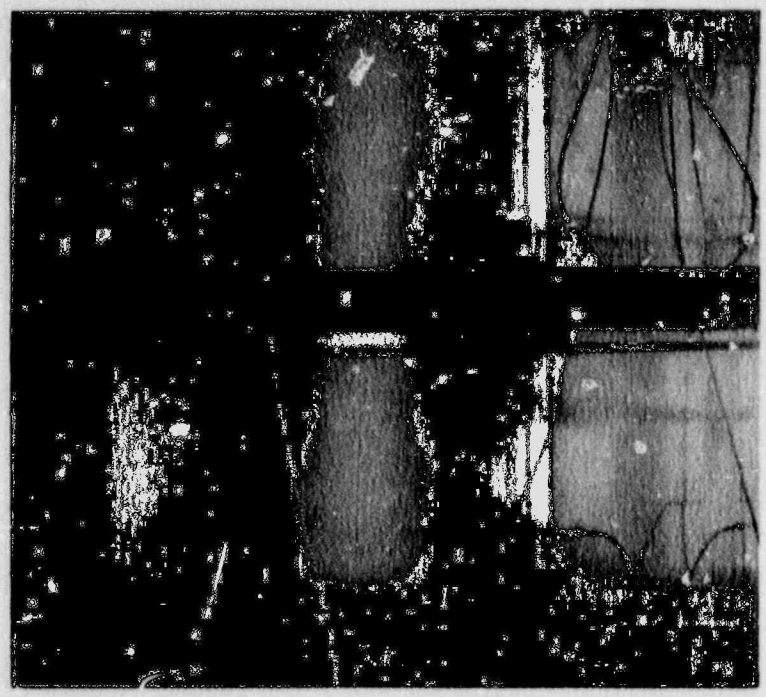

Fig. 12b. *The mixing phenomena in the VMR (partial entrainment at 480 gpm).*

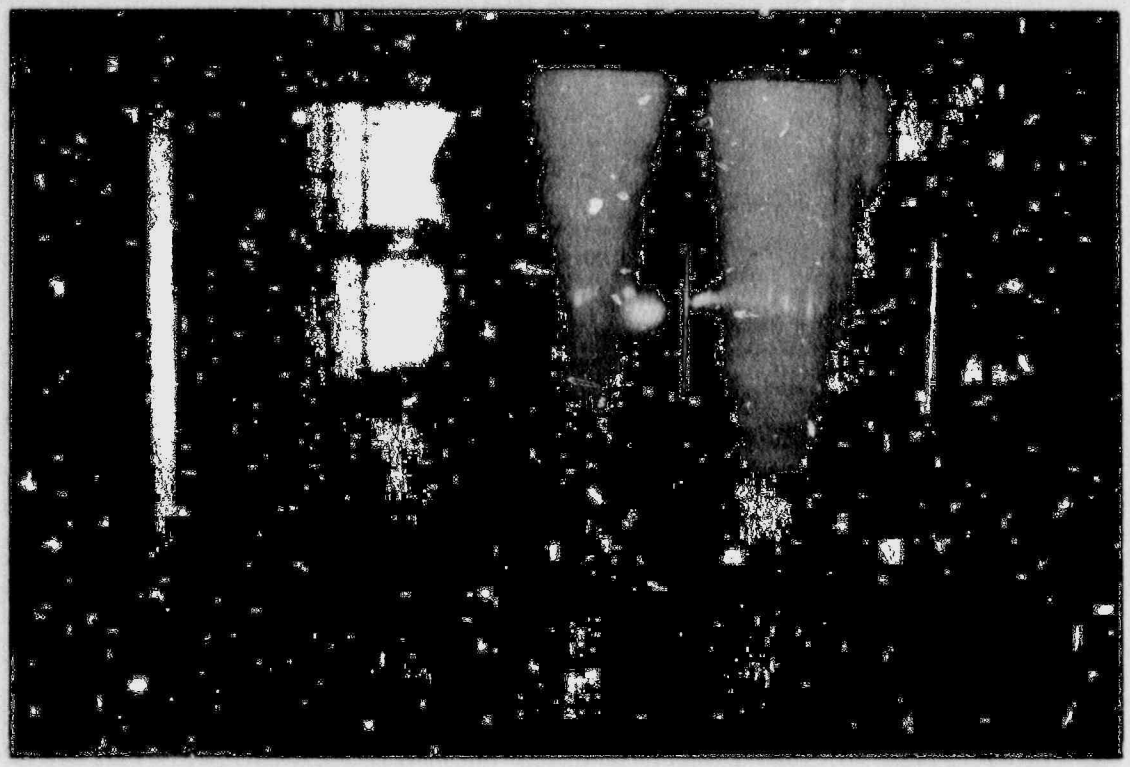

Fig. 13. *The mixing phenomena in the HMR.*

behavior are shown in Figures 14 and 15, respectively. The delay time (τ_d) indicated on these figures is the time required for a fluid particle to traverse from the lower injection nozzle to the outlet probe location at the mean flow rate. These data may be analyzed by means of a mass balance, as follows

$$V\frac{d\bar{\rho}}{dt} = \dot{Q}_R(\rho_i - \rho_o) + \dot{Q}_I(\rho_I - \rho_o), \tag{2}$$

where V is the volume of the subchannel space in the test section, $\dot{Q}_R$ and $\dot{Q}_I$ are the recirculating and injection flow rates, respectively, and ρ_i, ρ_o, and $\bar{\rho}$ are the inlet, outlet, and test section average densities, respectively. A rough indicator of the test section time constant can be obtained by setting $\bar{\rho} = \rho_o$, i.e.,

$$\tau = \frac{V}{\dot{Q}_R + \dot{Q}_I}. \tag{3}$$

This yields 12.4 s and 10.6 s (the delay times are within 1 s of these) for the runs of Figures 14 and 15, respectively. Thus, if the injected flow is fully entrained, steady state is obtained in a very short time, and Eq. (2) yields

$$\rho_o(\dot{Q}_R + \dot{Q}_I) = \rho_i\dot{Q}_R + \rho_I\dot{Q}_I. \tag{4}$$

Conversely, measured values of flows and densities can be substituted in Eq. (4) to determine the extent of departure from perfect mixing as reflected by the transient term in Eq. (2). Then

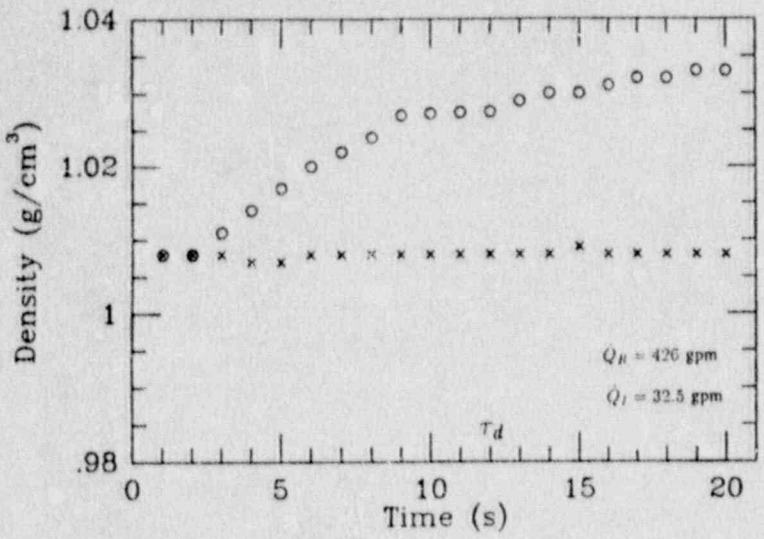

Fig. 14. *Inlet (x) and outlet (o) solute concentrations (3-nozzle injection).*

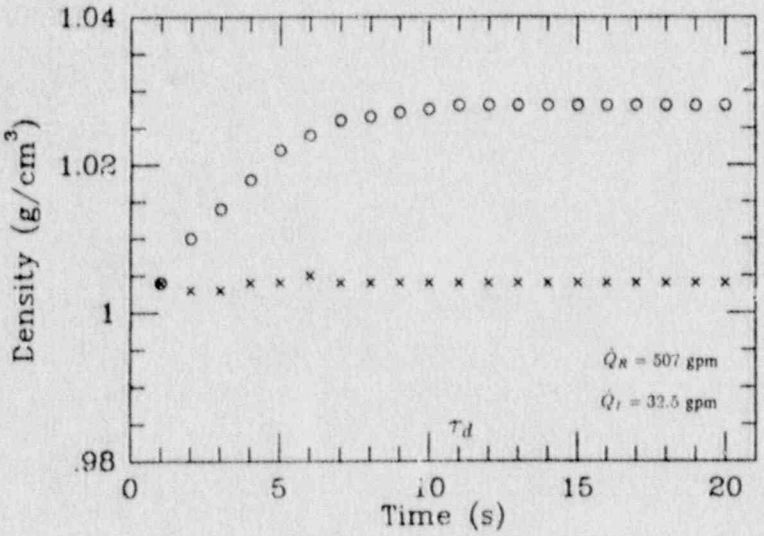

Fig. 15. *Inlet (x) and outlet (o) solute concentrations (3-nozzle injection).*

mixing efficiency can be defined as the fraction of injected salt mass that actually leaves the test section, i.e.,

$$\epsilon = \frac{\Delta\rho'_o}{\Delta\rho'_I} \quad \frac{\dot{Q}_R + \dot{Q}_I}{\dot{Q}_I}, \tag{5}$$

where

$$\Delta\rho'_o = \rho_o - \rho_i \quad \text{and} \quad \Delta\rho'_I = \rho_I - \rho_i. \tag{6}$$

Thus, each pair of measured densities (ρ_o, ρ_i) corresponds to a mixing efficiency, as shown in Figures 16 and 17 for the runs of Figures 14 and 15, respectively. The results for all the runs are given in the appendix.

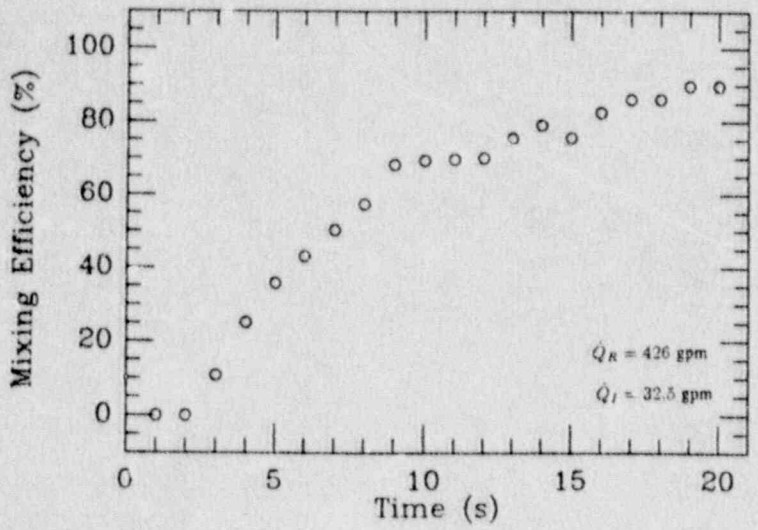

Fig. 16. *Mixing efficiency data for a run where entrainment is incomplete (3-nozzle injection).*

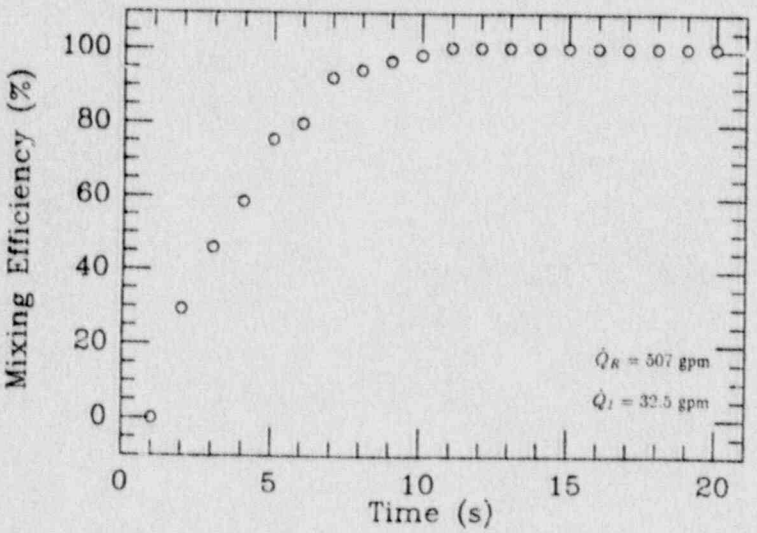

Fig. 17. *Mixing efficiency data for a typical fully-entraining run (3-nozzle injection).*

An interesting discriminating feature between complete and partial entrainment may be noted in these figures. In those runs that reflect complete entrainment, the mixing efficiency rises, within a few seconds, to a well-defined plateau. In contrast, for those runs characterized by partial entrainment, the mixing efficiency rises slowly and more or less uniformly for the duration of the run. This, of course, is expected as the accumulation term in Eq. (2) is now controlled by a significantly longer time constant ($\bar{\rho} \neq \rho_o$). Eventually, in this case also, 100% efficiency can be reached; however, this long term behavior is not of interest to the practical problem addressed here.

The short-term entrainment results from all runs are summarized in Figure 18. The efficiencies quoted here were obtained from the transient measurement of densities (ρ_i, ρ_o) at a

time equal to the delay time (τ_d) discussed above. The lower boundaries for perfect mixing for the three sets of experiments are obtained from Figure 18 (minimum values of $\dot{Q}_R$ at which $\epsilon = 100\%$ (using a least squares linear fit)) are summarized in Figure 19. The prototypic $\Delta\rho/\rho_I$ value is 0.355, which, using a least squares linear fit and Figure 19, yields 583 gpm (~8.2% of rated) as the lower boundary of the full entrainment regime for 3-nozzle injection. This value of lower boundary agrees very well with the value, obtained using Froude scaling ($U \propto \sqrt{\Delta\rho/\rho_I}$), of 557 gpm (7.8% of rated). In combination with the HMR, we believe that the actual threshold is considerably lower than 8.2%. What remains to be done is to establish such trends as a function of the number of injection nozzles (up to seven) and subject the imperfectly mixed ranges to the horizontal mixing regime. Also, we plan to consider the effect of higher injection flow rates since such, perhaps in combination with enriched boron, could be quite beneficial in achieving rapid shutdown.

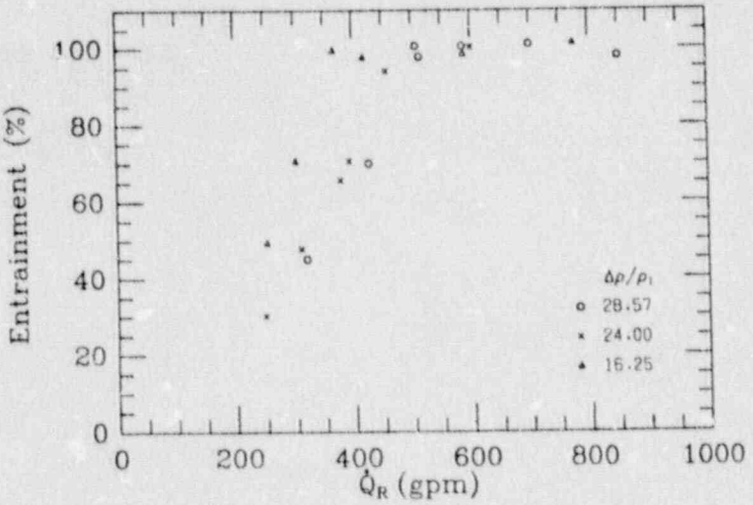

Fig. 18. *The variation of % entrainment with recirculation flow rate (3-nozzle injection).*

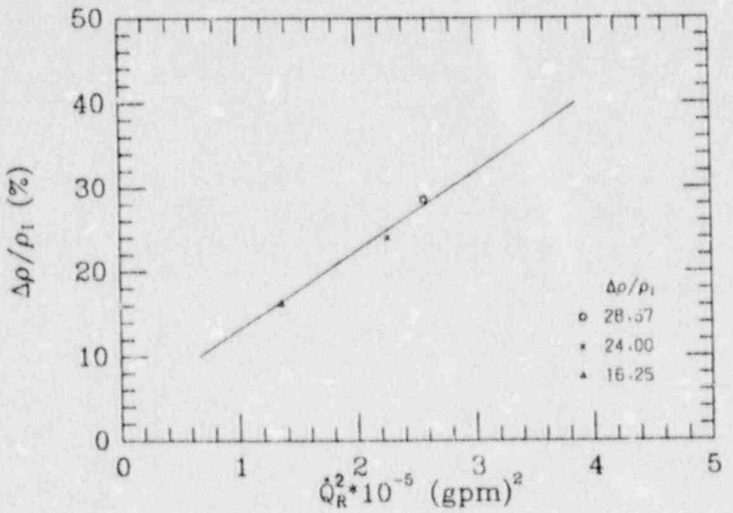

Fig. 19. *The variation of $\Delta\rho/\rho_I$ with recirculation flow rate (3-nozzle injection).*

5. CONCLUSIONS AND RECOMMENDATIONS

So far we have established a scaling rational and an experimental approach to assess boron mixing in the lower plenum of a BWR during ATWS. We have determined that with a three-hole injection full entrainment occurs at natural circulation flow of ~8.2% of rated. Clearly, it is important to pursue the effects of nozzle number (up to 7), and the multidimensional flows in the partially entraining regime. The latter will provide the boundary conditions for exploring the secondary entrainment in the horizontal mixing regime. Based on what we have seen, we believe it will be possible to demonstrate perfect mixing for the practical situation of interest under ATWS and to eventually effect a change of operator procedures to the benefit of real as well as perceived safety.

REFERENCES

1. BWR Owner's Group letter to the U.S. Nuclear Regulatory Commission, February 1982.
2. Chexal et al., NSAC/69, Electric Power Research Institute, May 1984.
3. T.G. Theofanous et al., "Decay of Buoyancy Driven Stratified Layer with Applications to Pressurized Thermal Shock (PTS)," NUREG/CR- 3700, February 1984.

APPENDIX

DETAILED EXPERIMENTAL RESULTS

This appendix contains the experimental data from all runs performed so far. The table below gives the conditions for each and the key result, i.e., the % entrainment. This table is also used as a key to the figures that follow; Fig. x-y(z) means: x is the set number (I, II, or III), y is the run number (1 to 19), and (z) is set to (a) for figures presenting measured inlet and outlet concentrations, and to (b) for figures presenting deduced entrainment transients. The delay time τ_d has been defined on page 12, and the entrainment shown in the table is read off these figures for time (from the start of the run) equal to this delay time.

As mentioned in the body of the report, all these runs were made with $CaC\ell_2$ and using 3-nozzle injections (nozzles number 3, 4, and 5).

TABLE A.1

Experimental Test Matrix

Set #	Run #	ρ_I (g/cm^3)	$\Delta\rho/\rho_I$ (%)	$\dot{Q}_R$ (gpm)	$\dot{Q}_I$ (gpm)	τ_d (s)	% Entrainment at τ_d
	1			318	32.5	16	45
	2			426	32.5	12	70
	3			507	32.5	11	100
I	4	1.4	28.57	513	32.5	10	98
	5			586	32.5	9	100
	6			700	32.5	8	100
	7			850	32.5	6	98
	8			248	30.2	20	30
	9			309	30.2	17	48
	10			378	30.2	14	66
II	11	1.316	24.00	393	30.2	13	71
	12			457	30.2	12	94
	13			600	30.2	9	100
	14			252	29.8	20	49
	15			301	29.8	18	71
	16			367	29.8	14	100
III	17	1.194	16.25	419	29.8	13	98
	18			588	29.8	9	99
	19			775	29.8	7	100

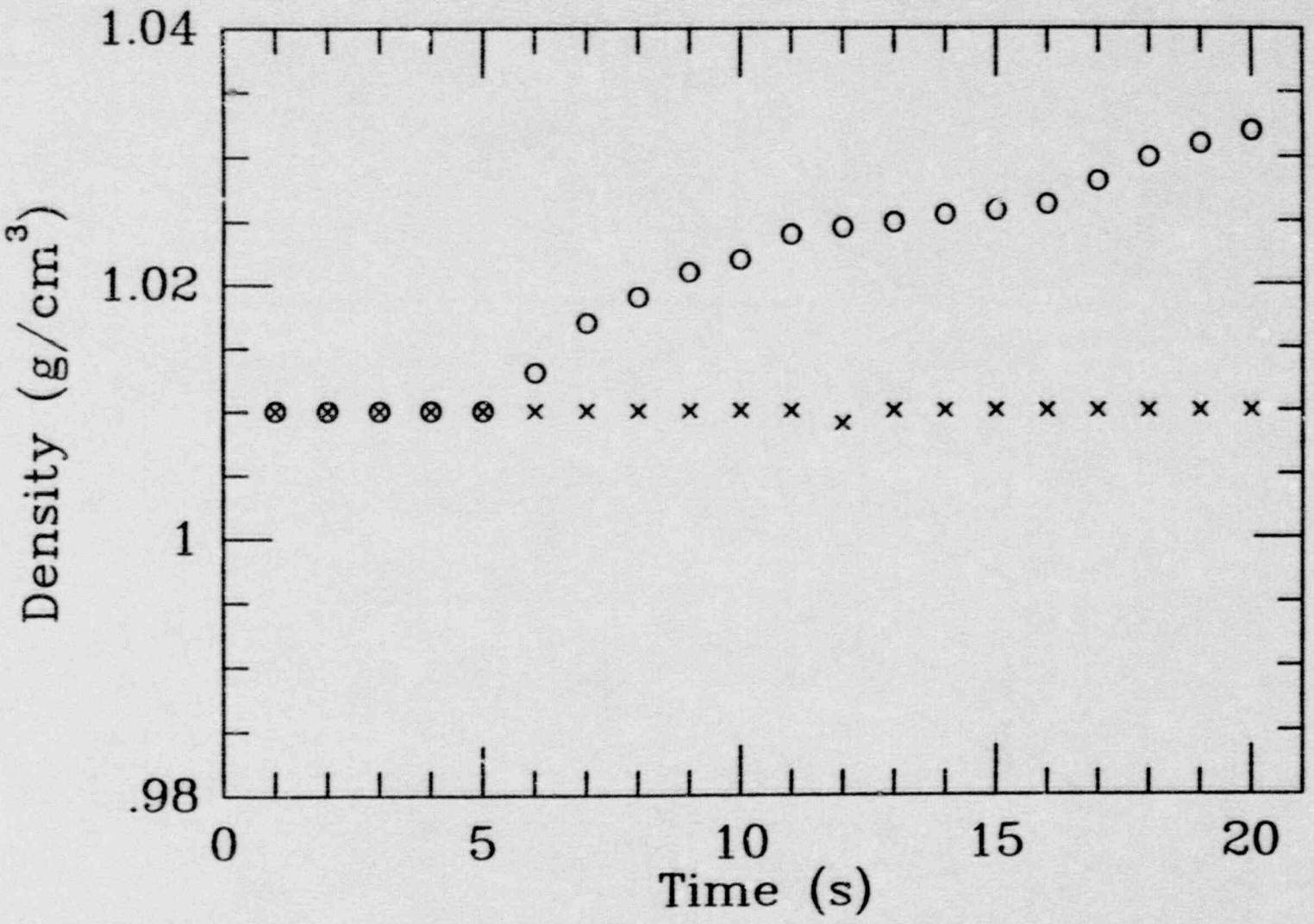

Fig. I-1a. *Inlet (x) and outlet (o) solute concentrations (partial entrainment).*

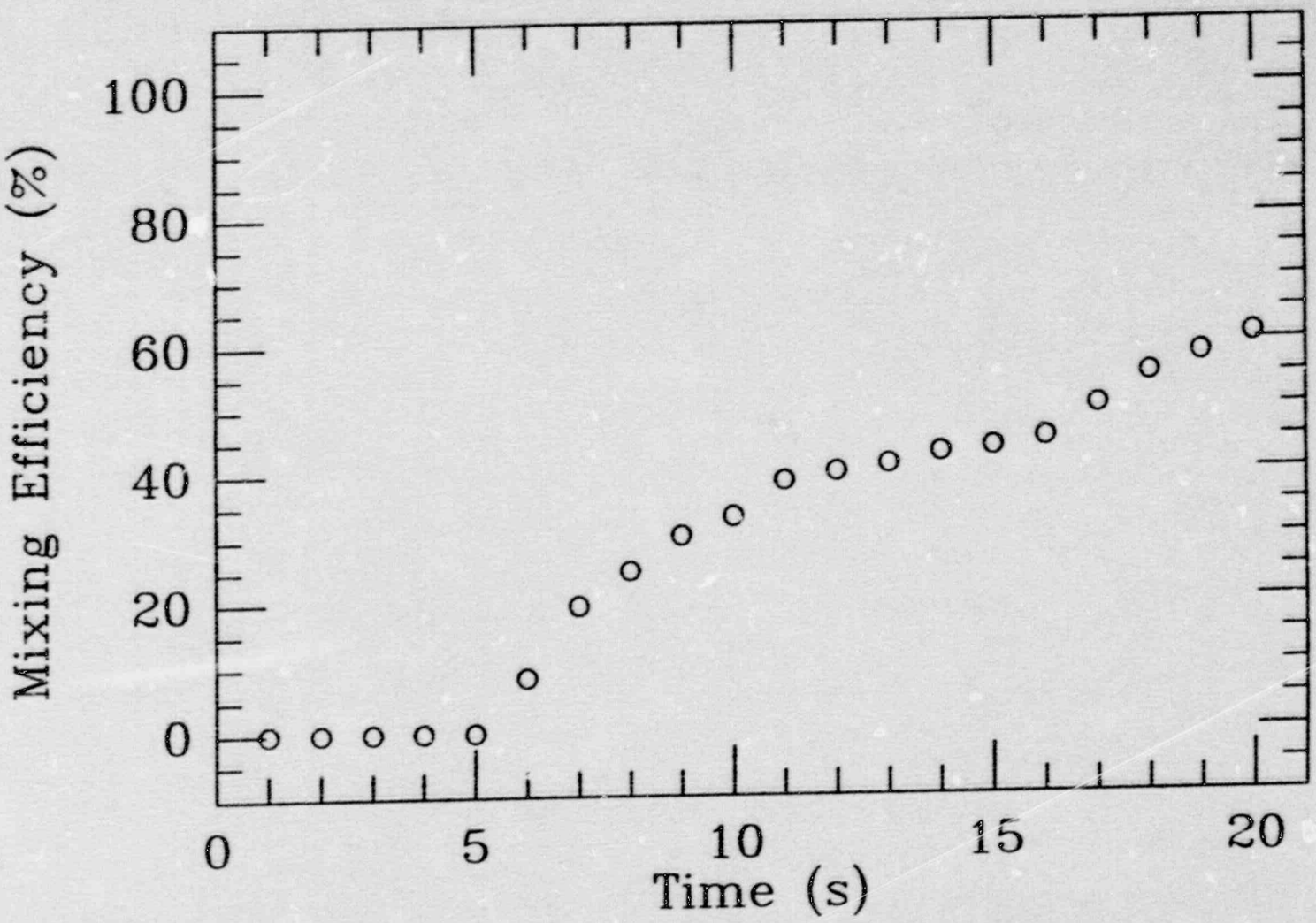

Fig. I-1b. *Mixing efficiency data (partial entrainment).*

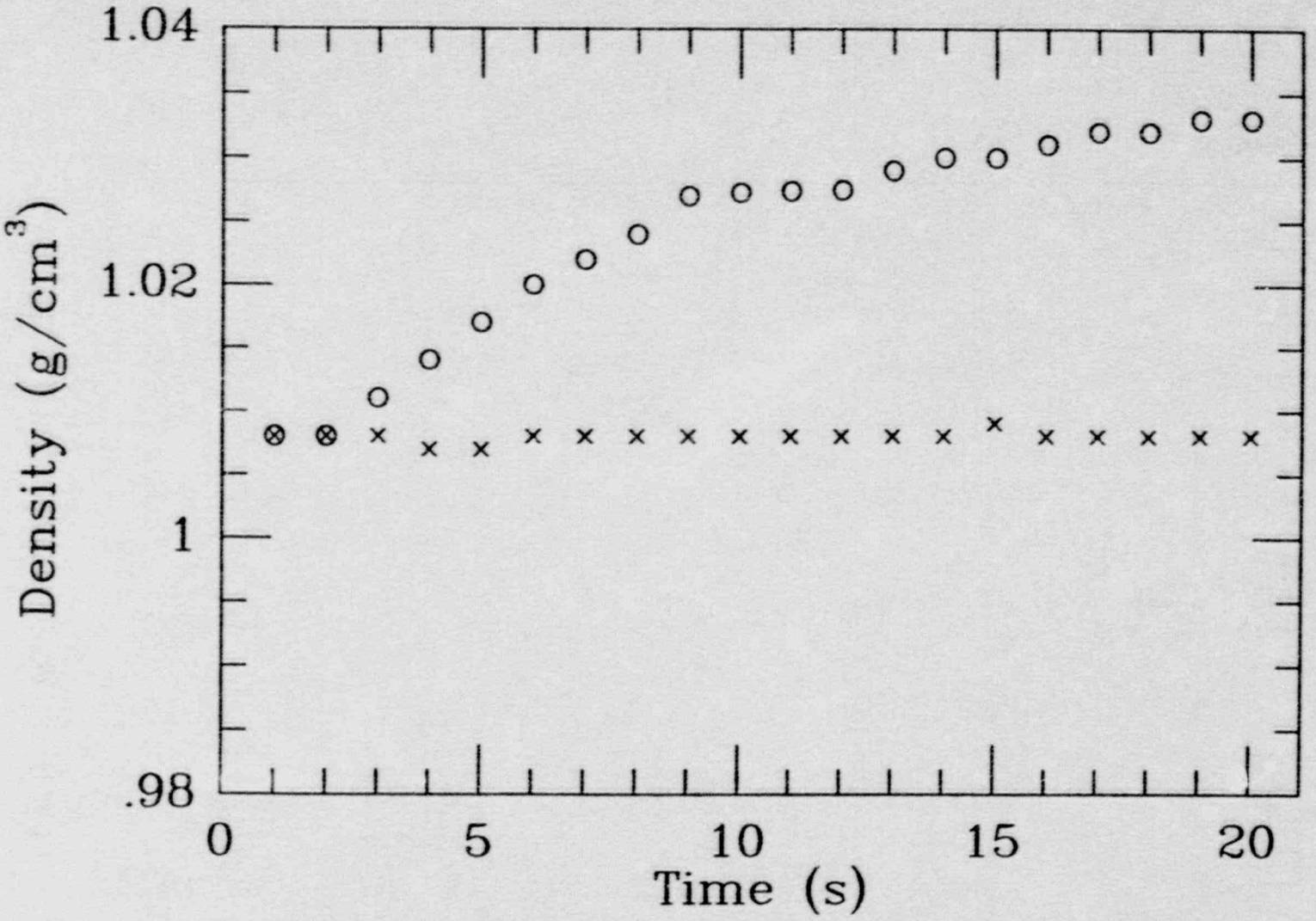

Fig. I-2a. *Inlet (x) and outlet (o) solute concentrations (partial entrainment).*

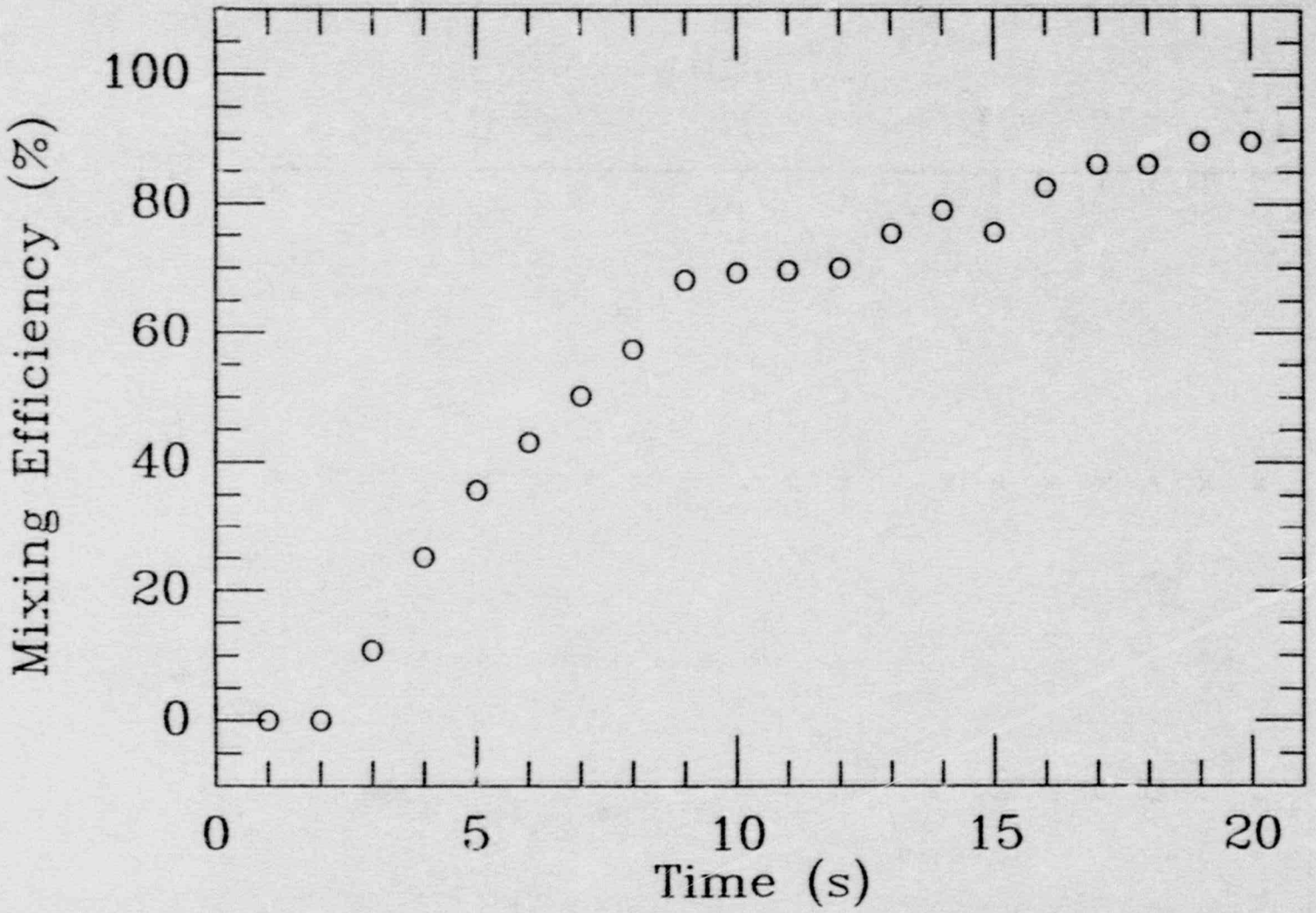

Fig. 1-2b. *Mixing efficiency data (partial entrainment).*

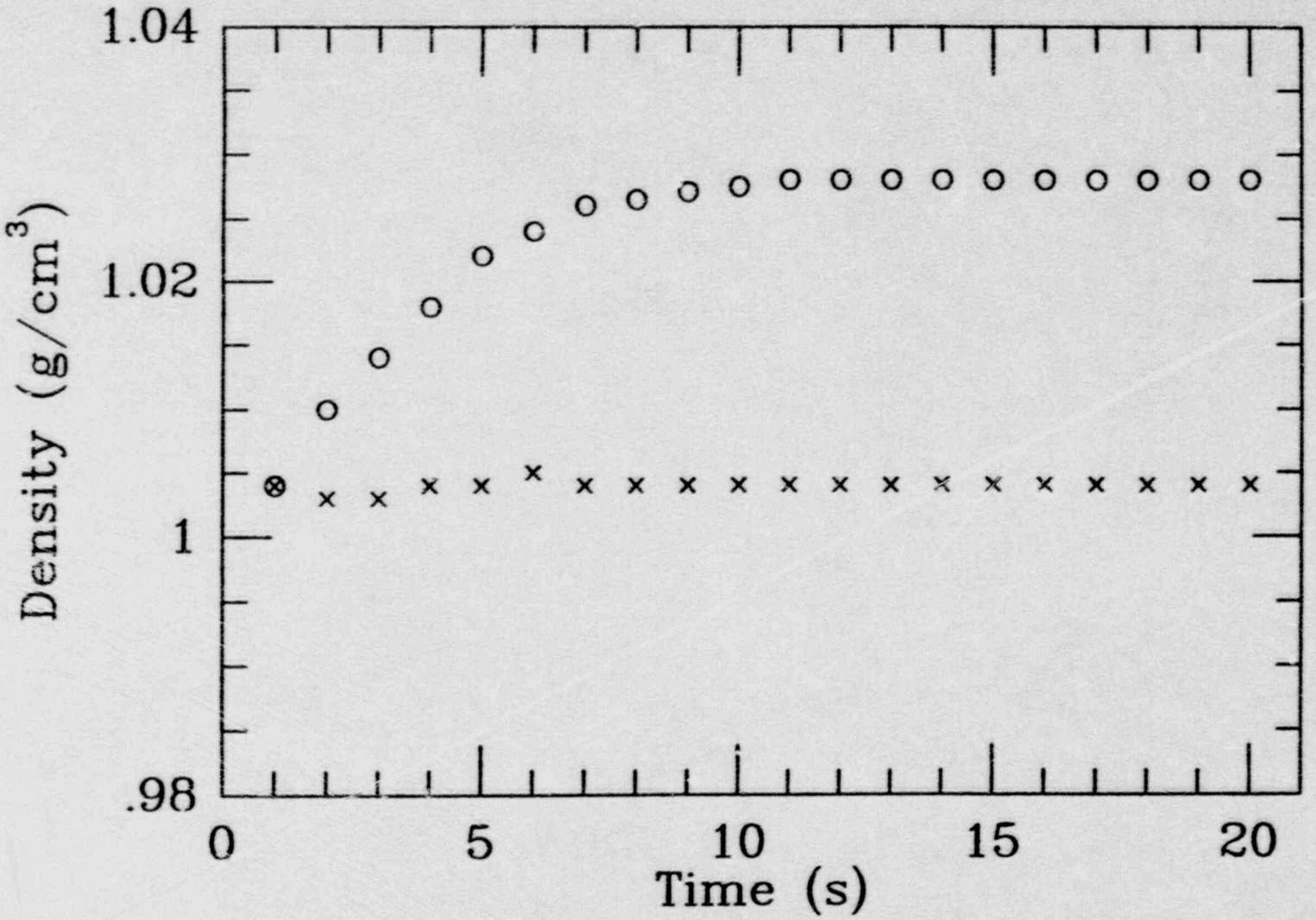

Fig. I-3a. *Inlet (x) and outlet (o) solute concentrations (full entrainment).*

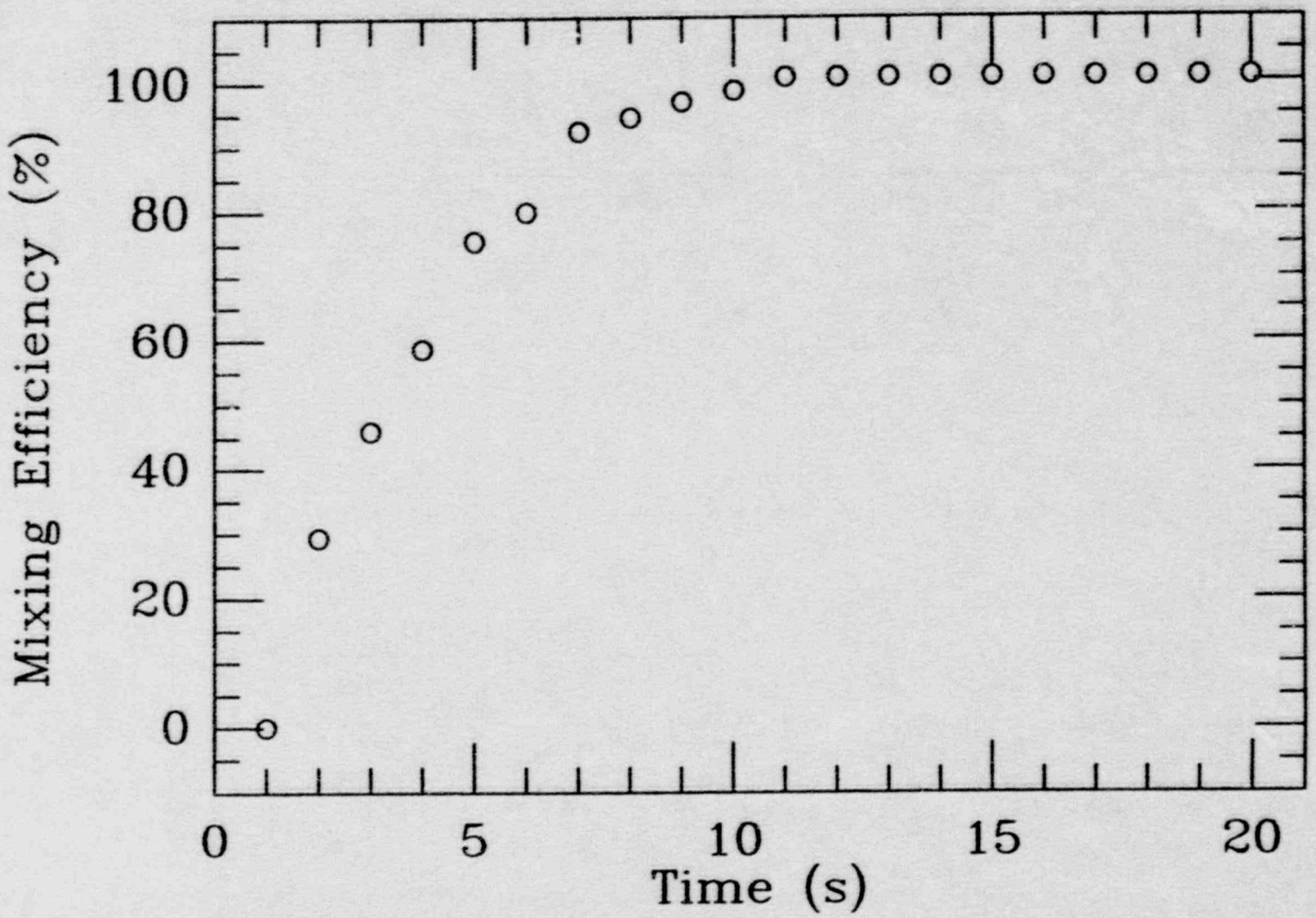

Fig. I-3b. *Mixing efficiency data (full entrainment).*

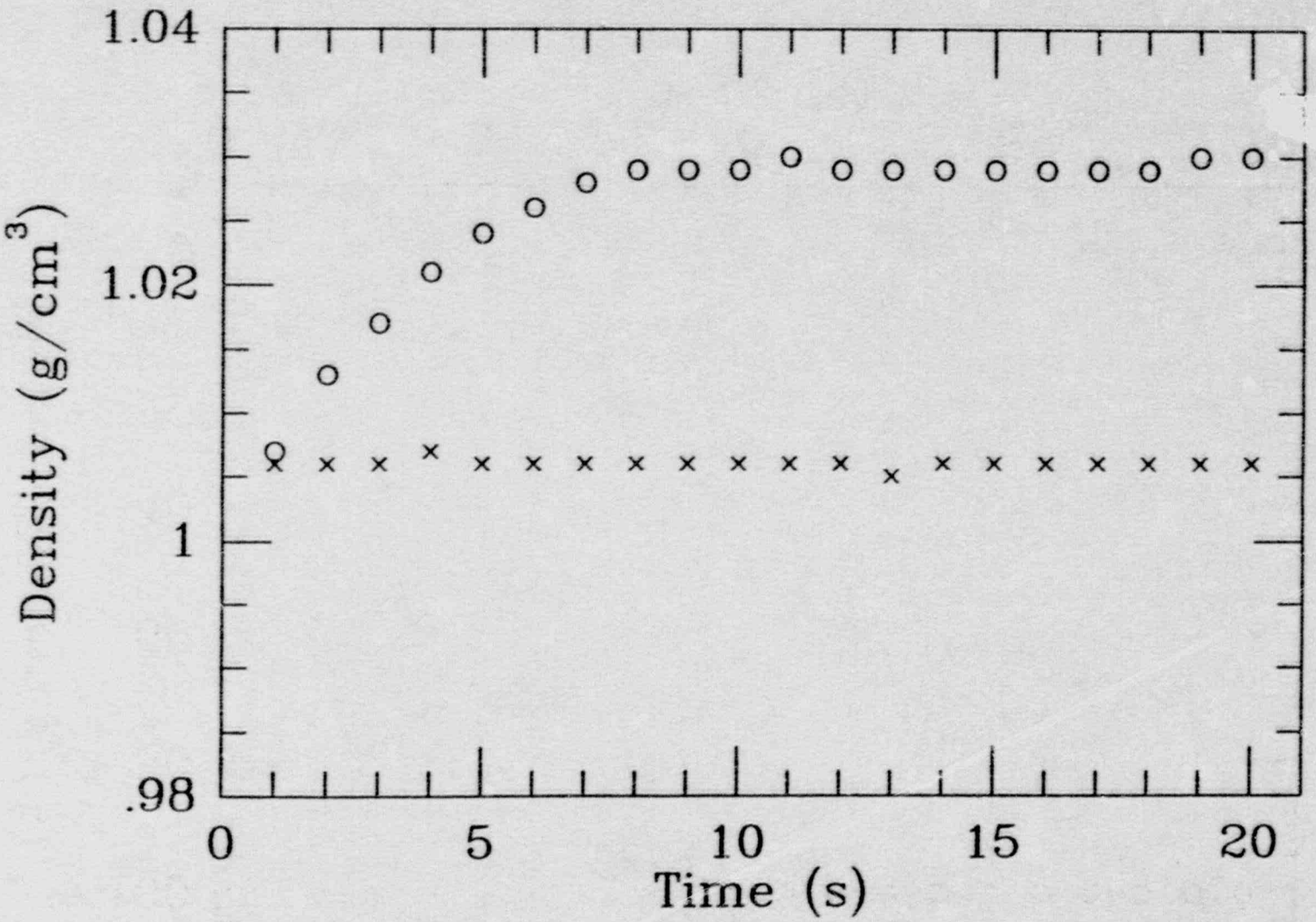

Fig. I-4a. *Inlet (x) and outlet (o) solute concentrations (full entrainment).*

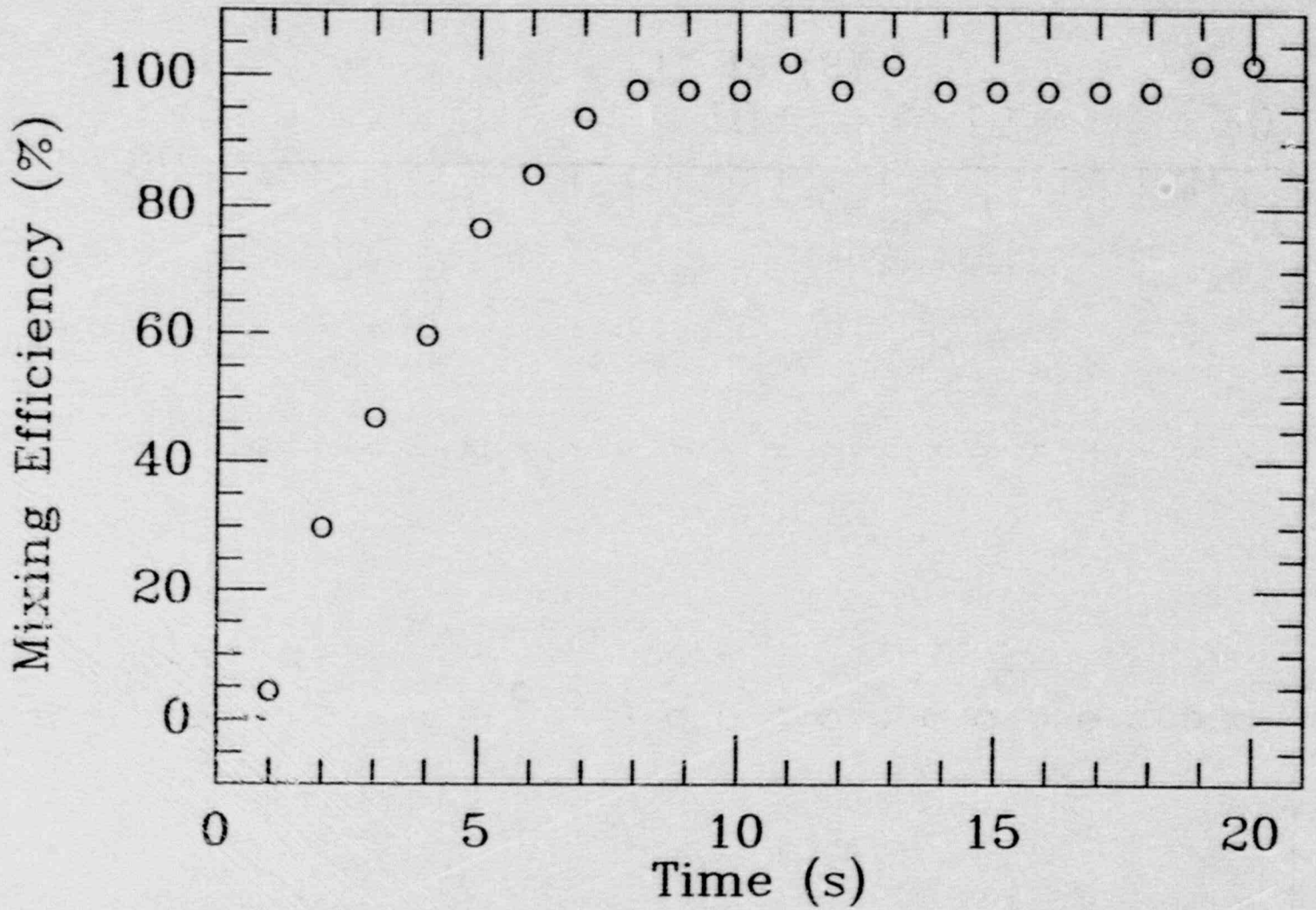

Fig. I-4b. *Mixing efficiency data (full entrainment).*

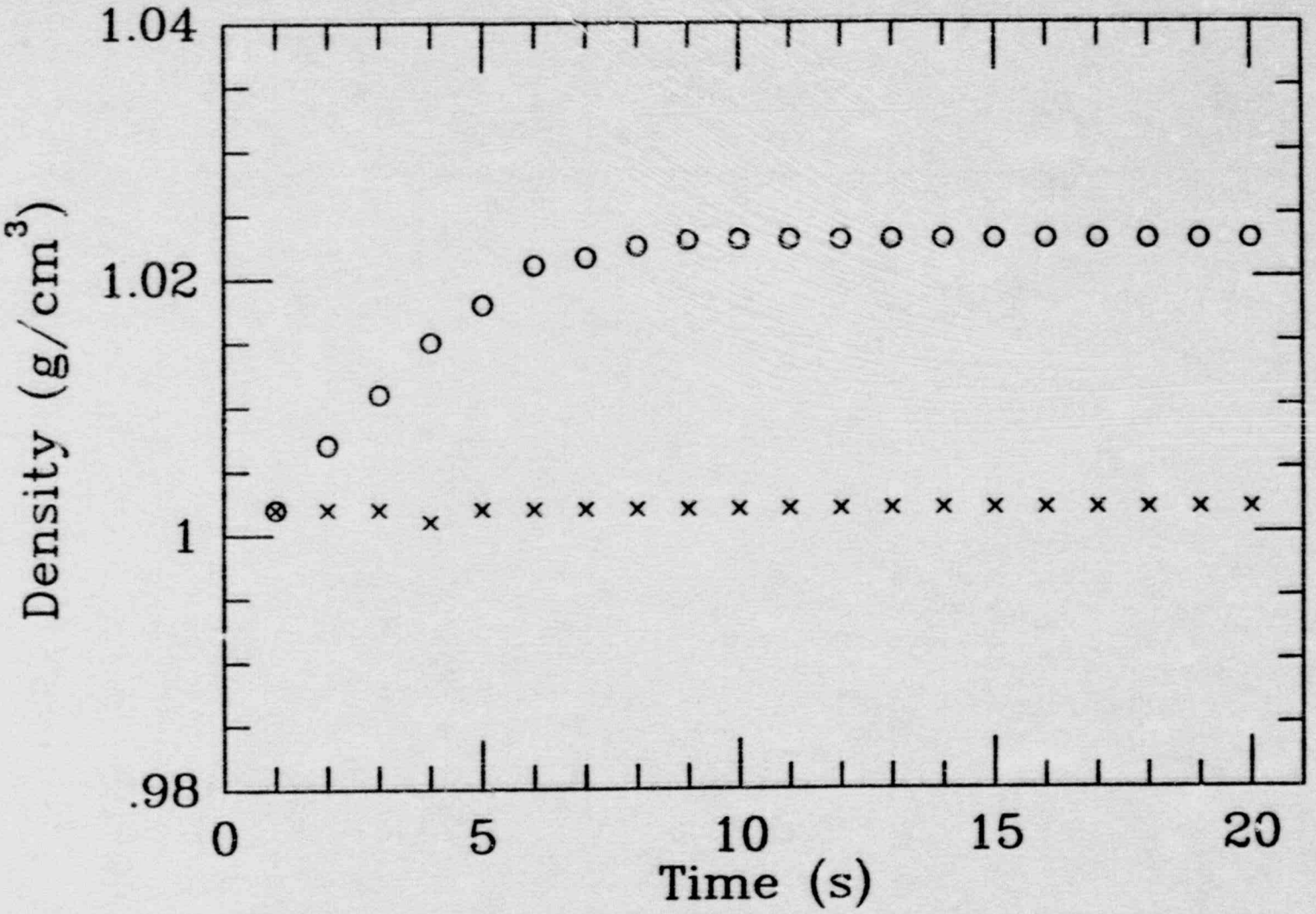

Fig. I-5a. *Inlet (x) and outlet (o) solute concentrations (full entrainment).*

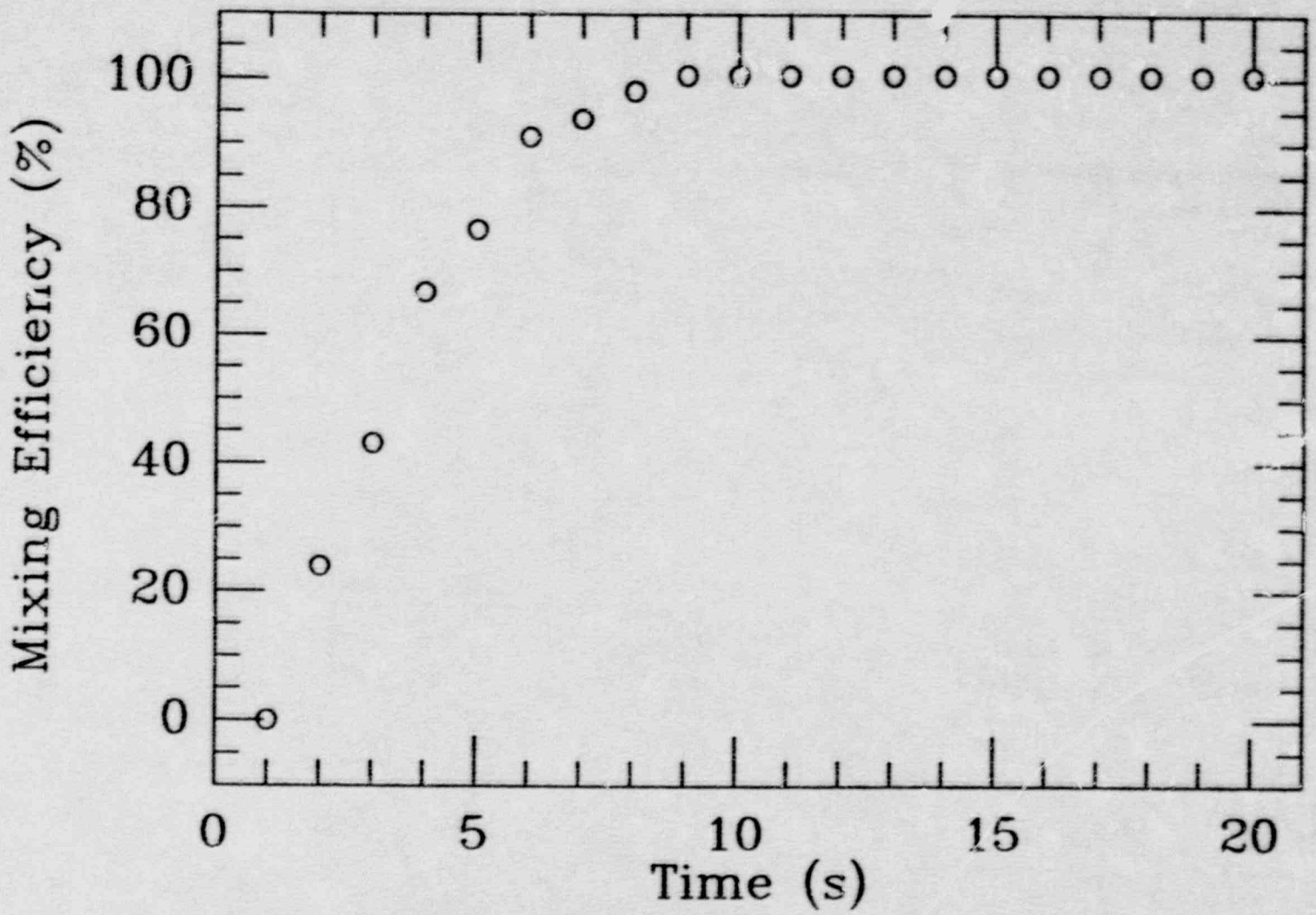

Fig. I-5b. *Mixing efficiency data (full entrainment).*

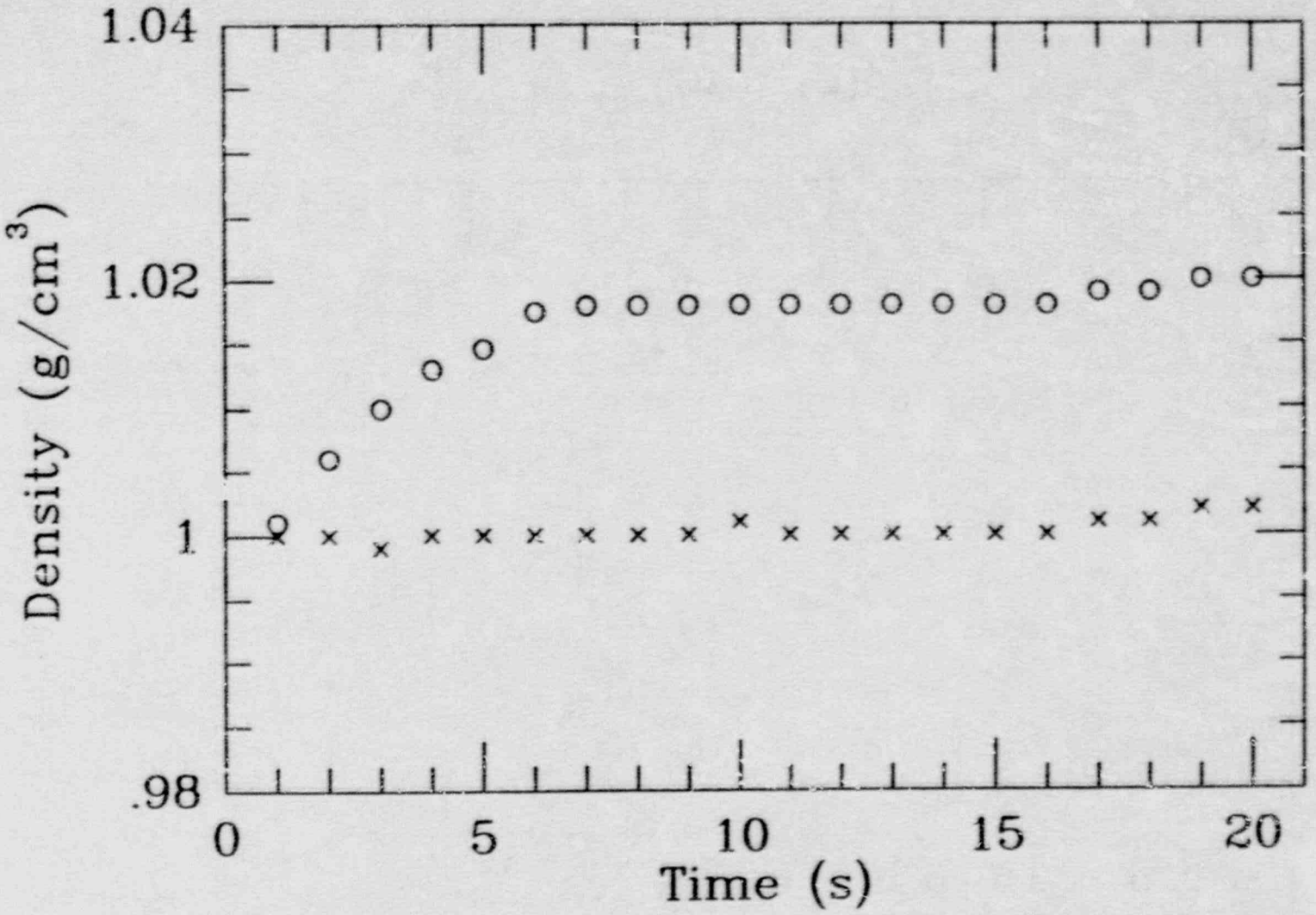

Fig. I-6a. *Inlet (x) and outlet (o) solute concentrations (full entrainment).*

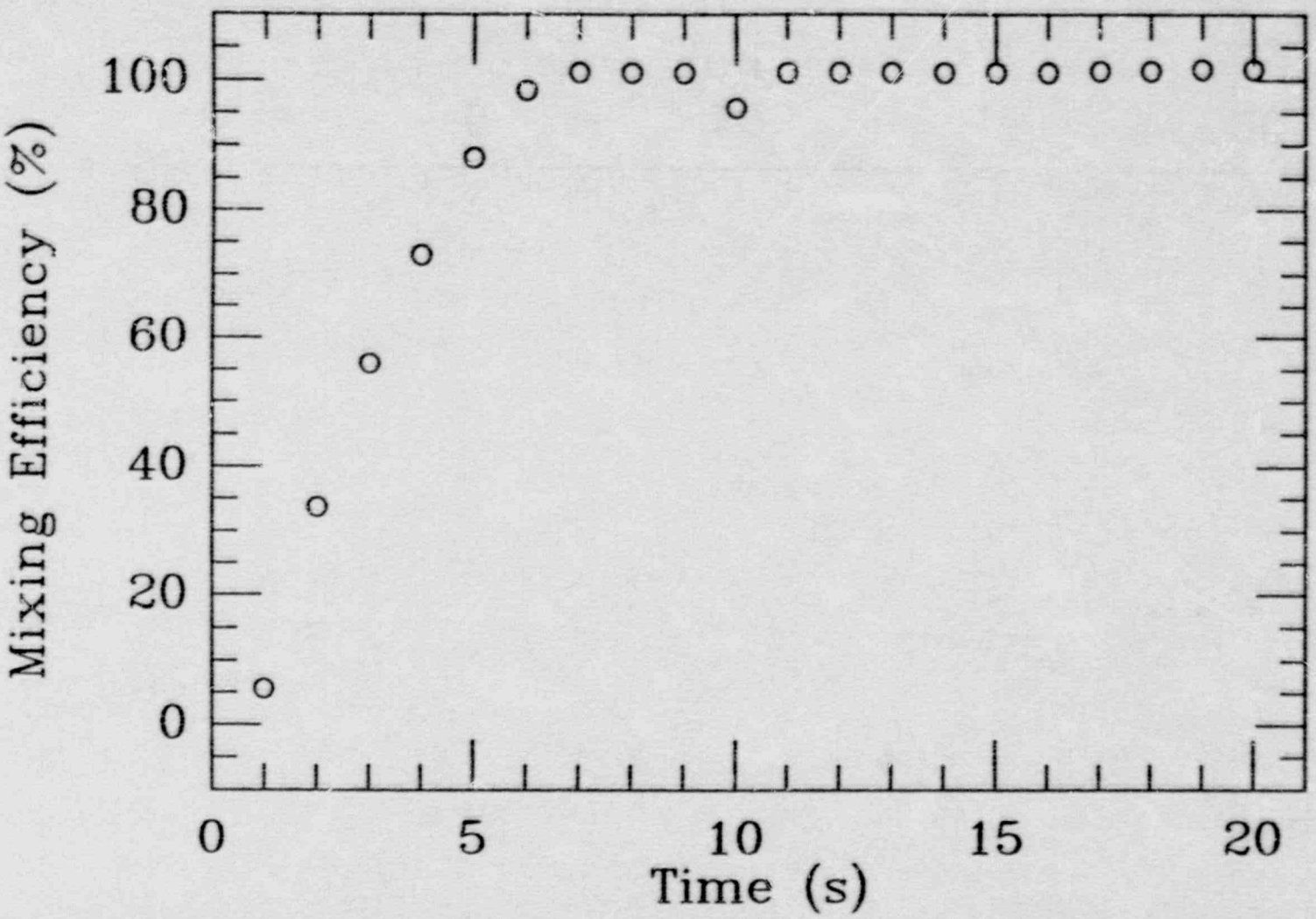

Fig.*I-6b. Mixing efficiency data (full entrainment).*

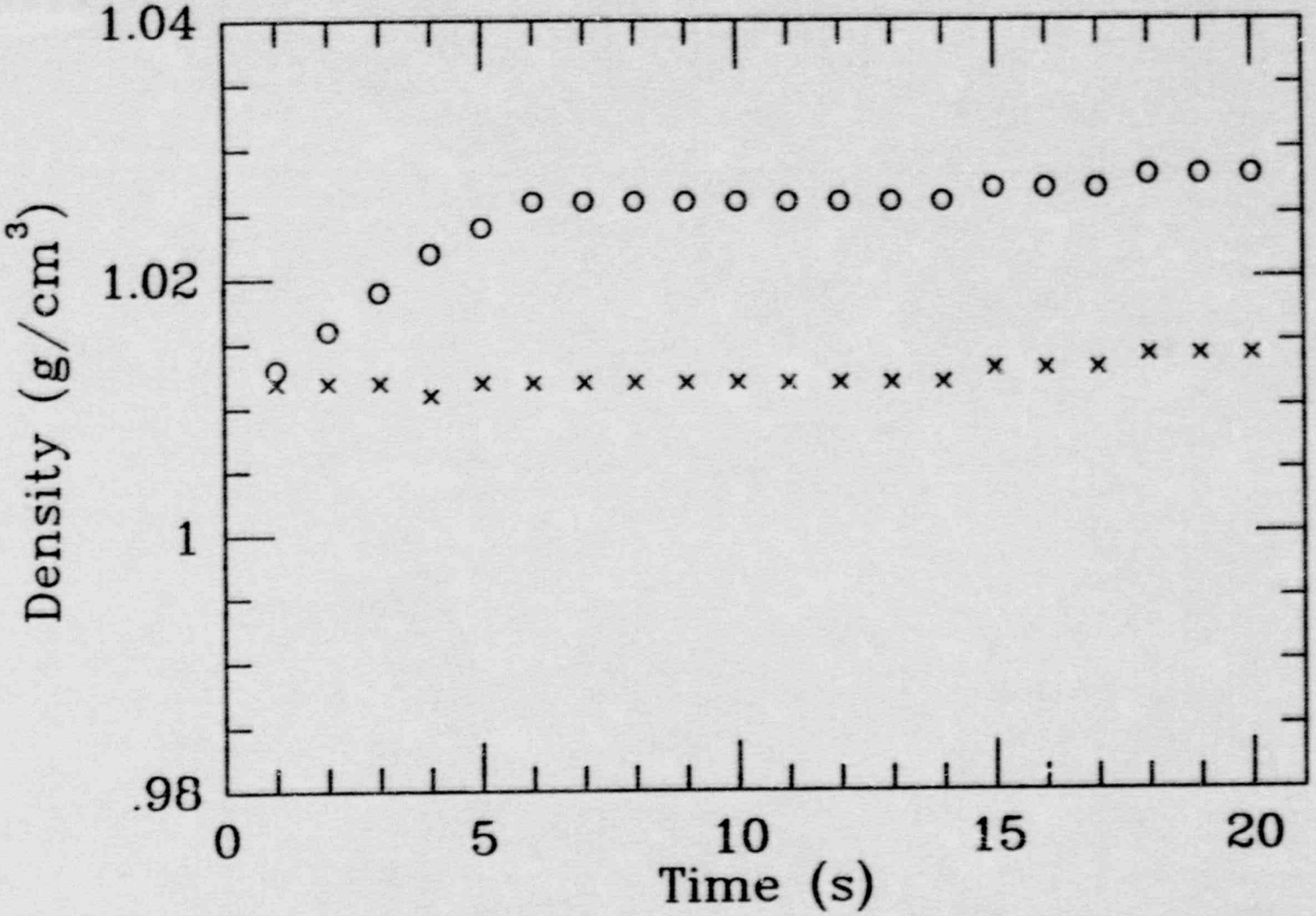

Fig. I-7a. *Inlet (x) and outlet (o) solute concentrations (full entrainment).*

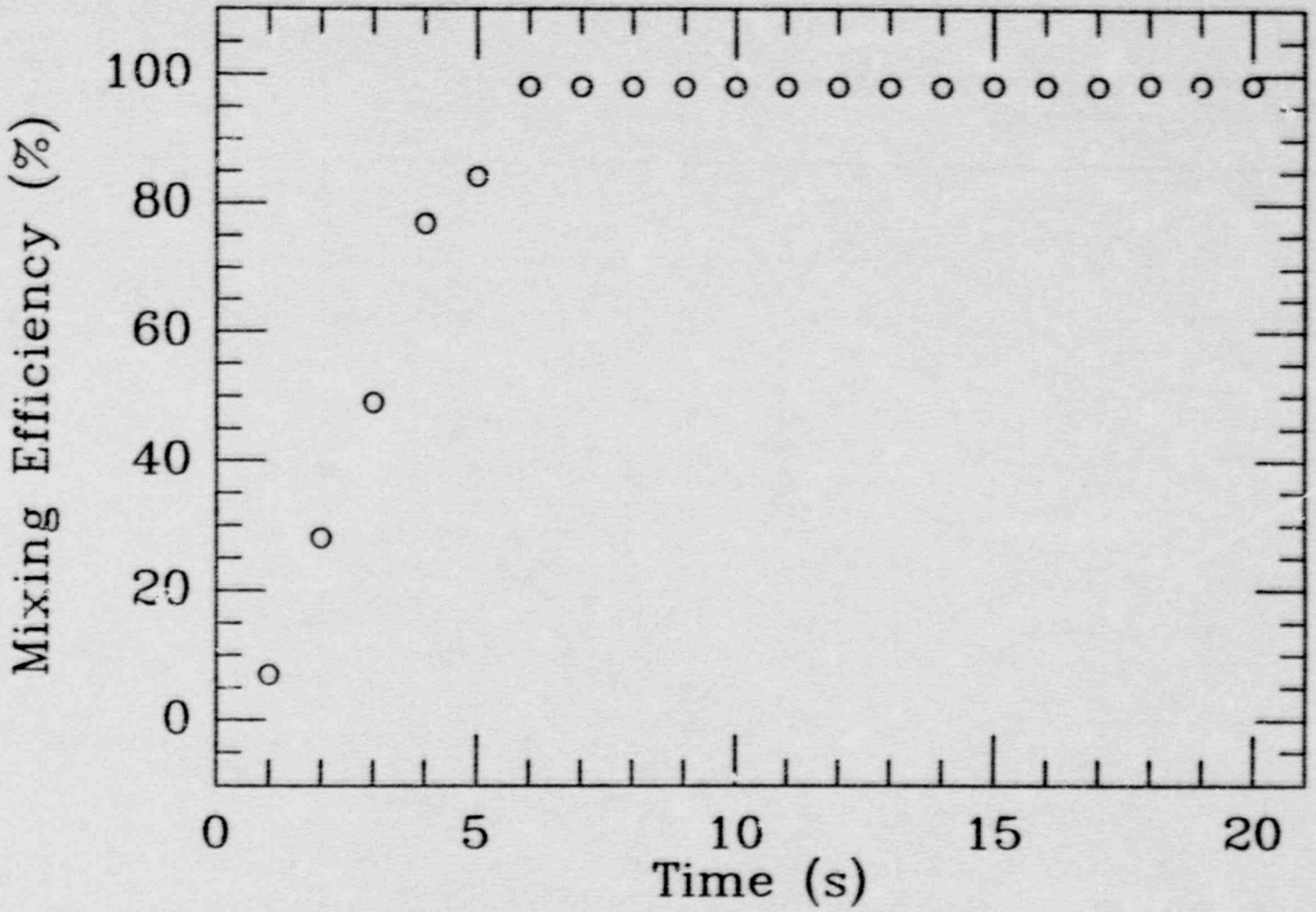

Fig. I-7b. *Mixing efficiency data (full entrainment).*

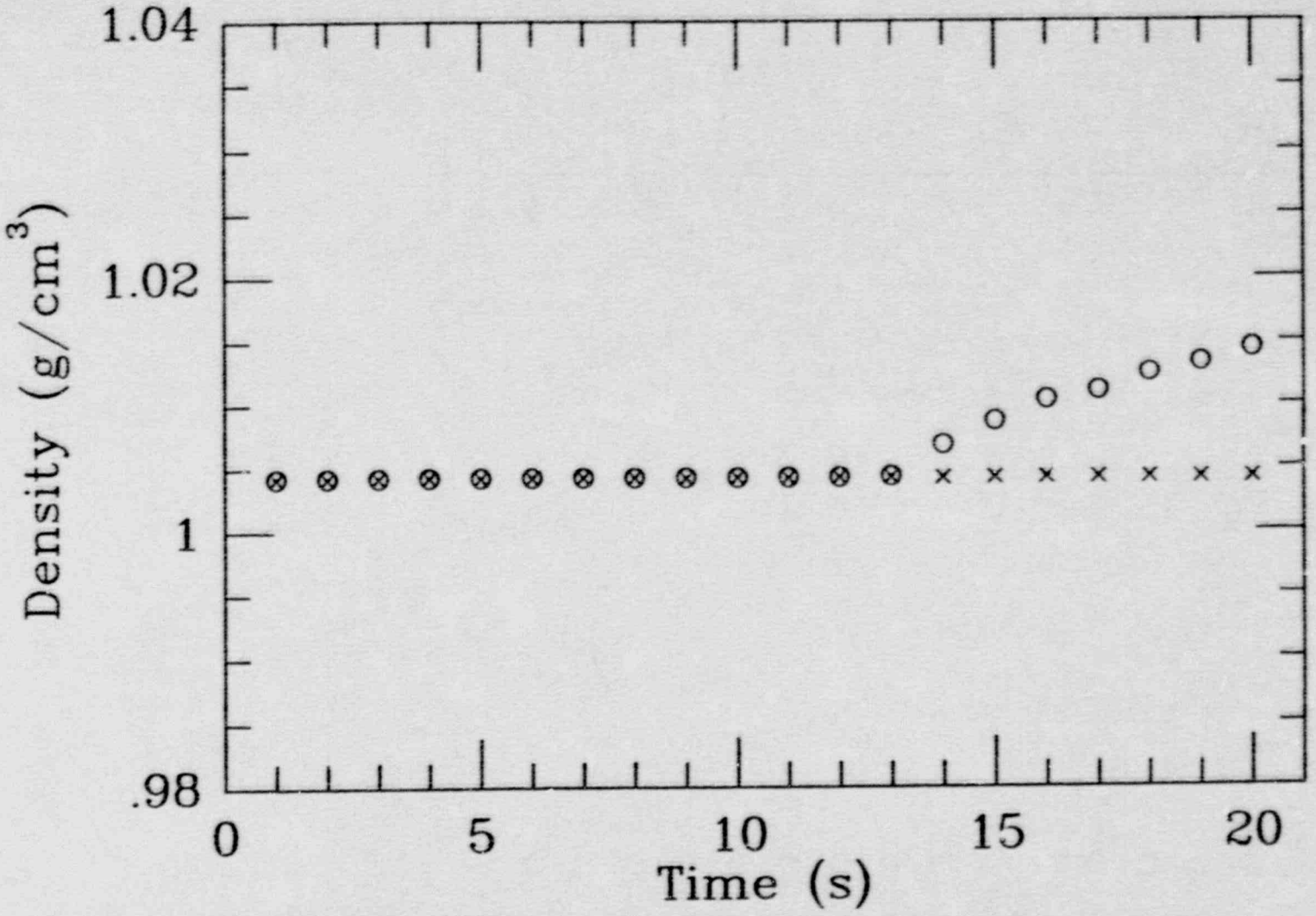

Fig. II-8a. *Inlet (x) and outlet (o) solute concentrations (partial entrainment).*

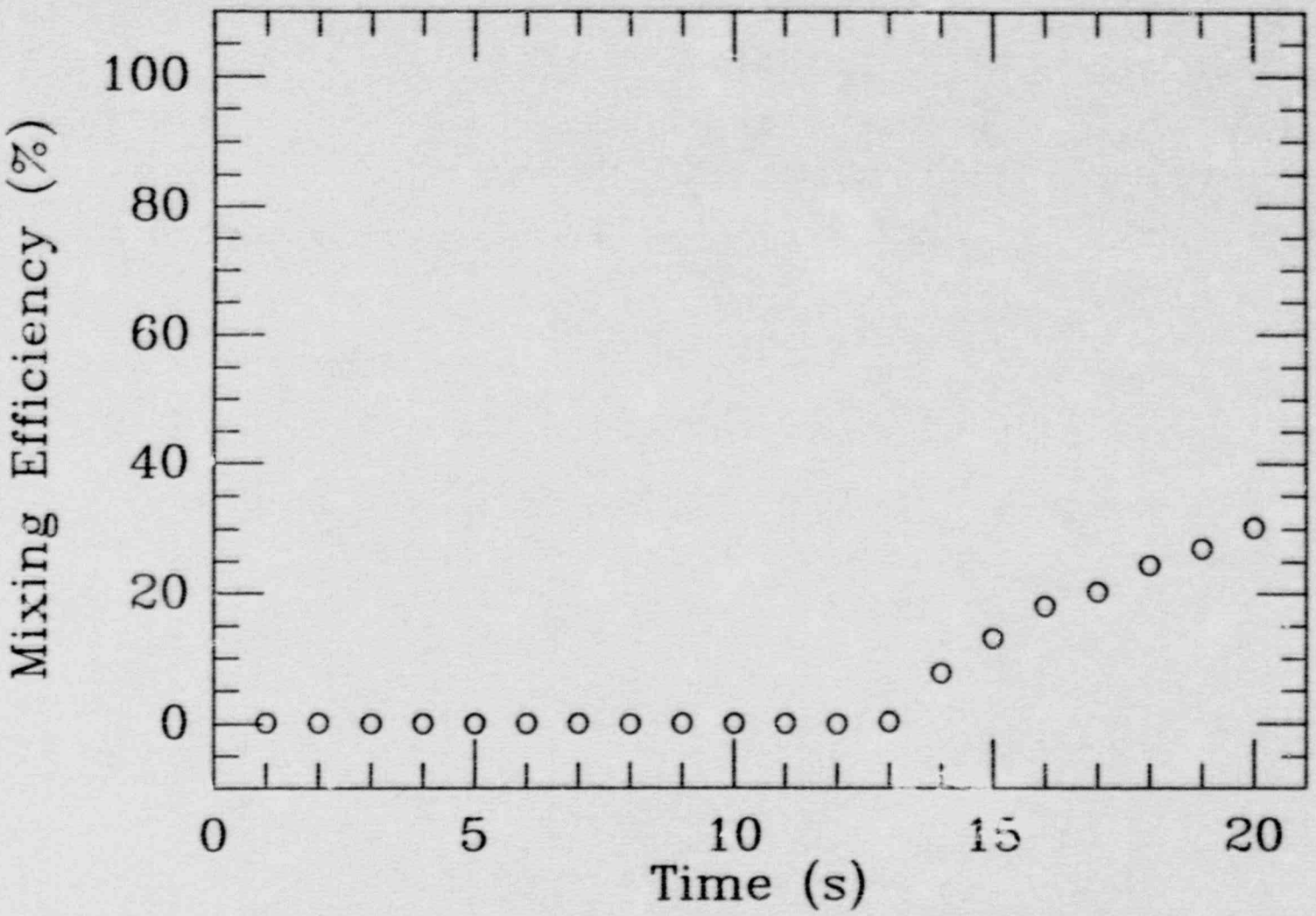

Fig. II-8b. *Mixing efficiency data (partial entrainment).*

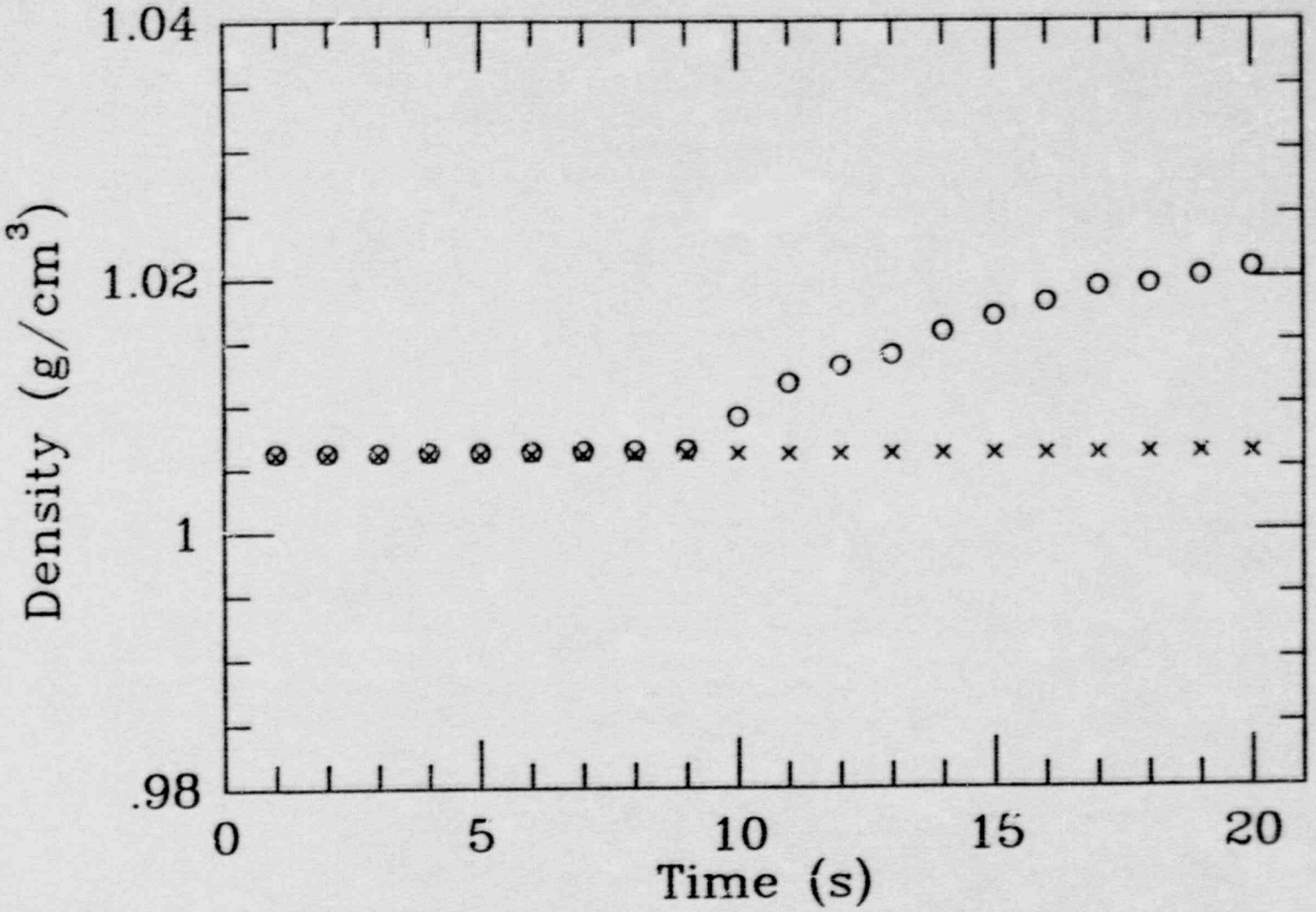

Fig. II-9a. *Inlet (x) and outlet (o) solute concentrations (partial entrainment).*

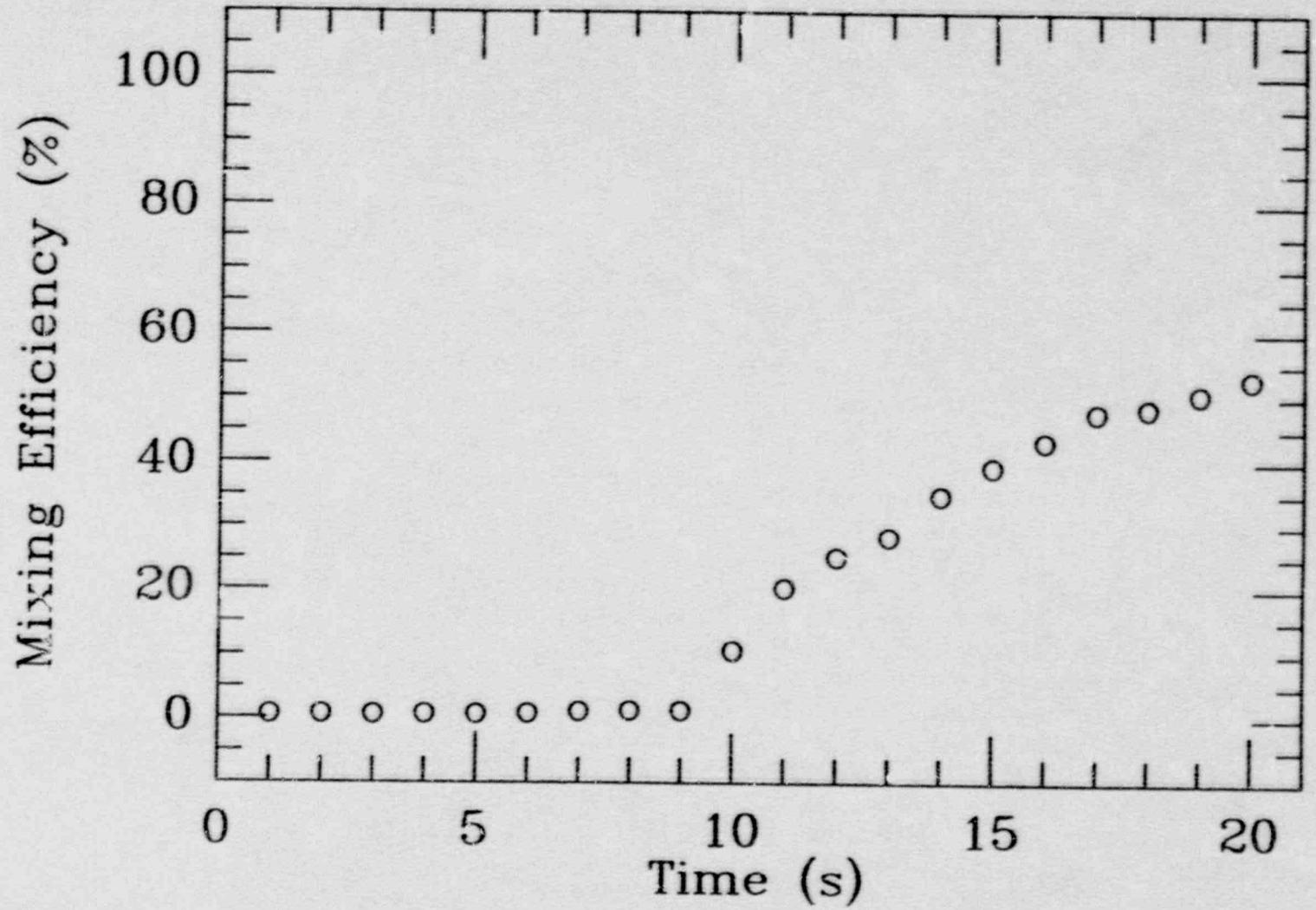

Fig. II-9b. *Mixing efficiency data (partial entrainment).*

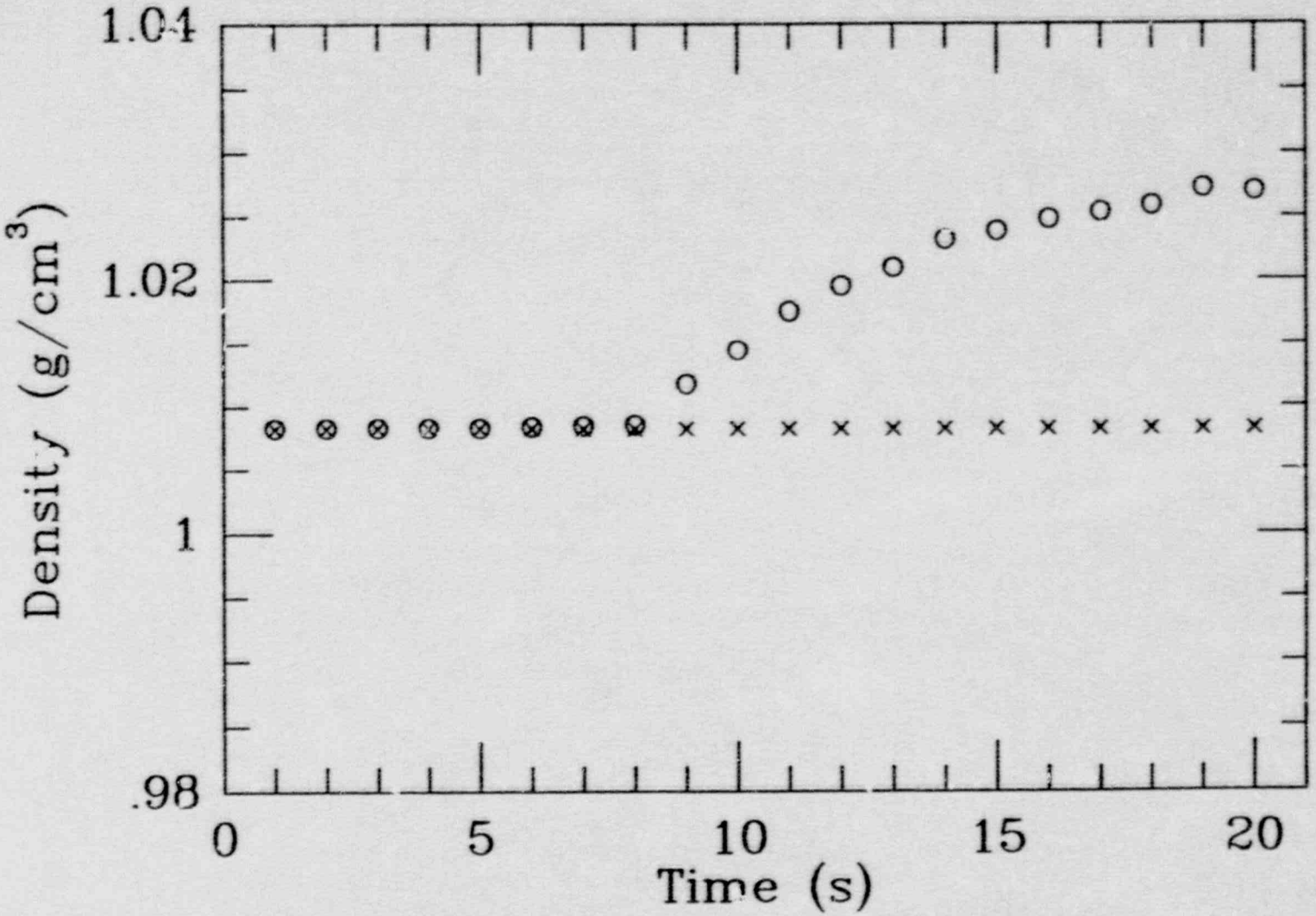

Fig. II-10a. *Inlet (x) and outlet (o) solute concentrations (partial entrainment).*

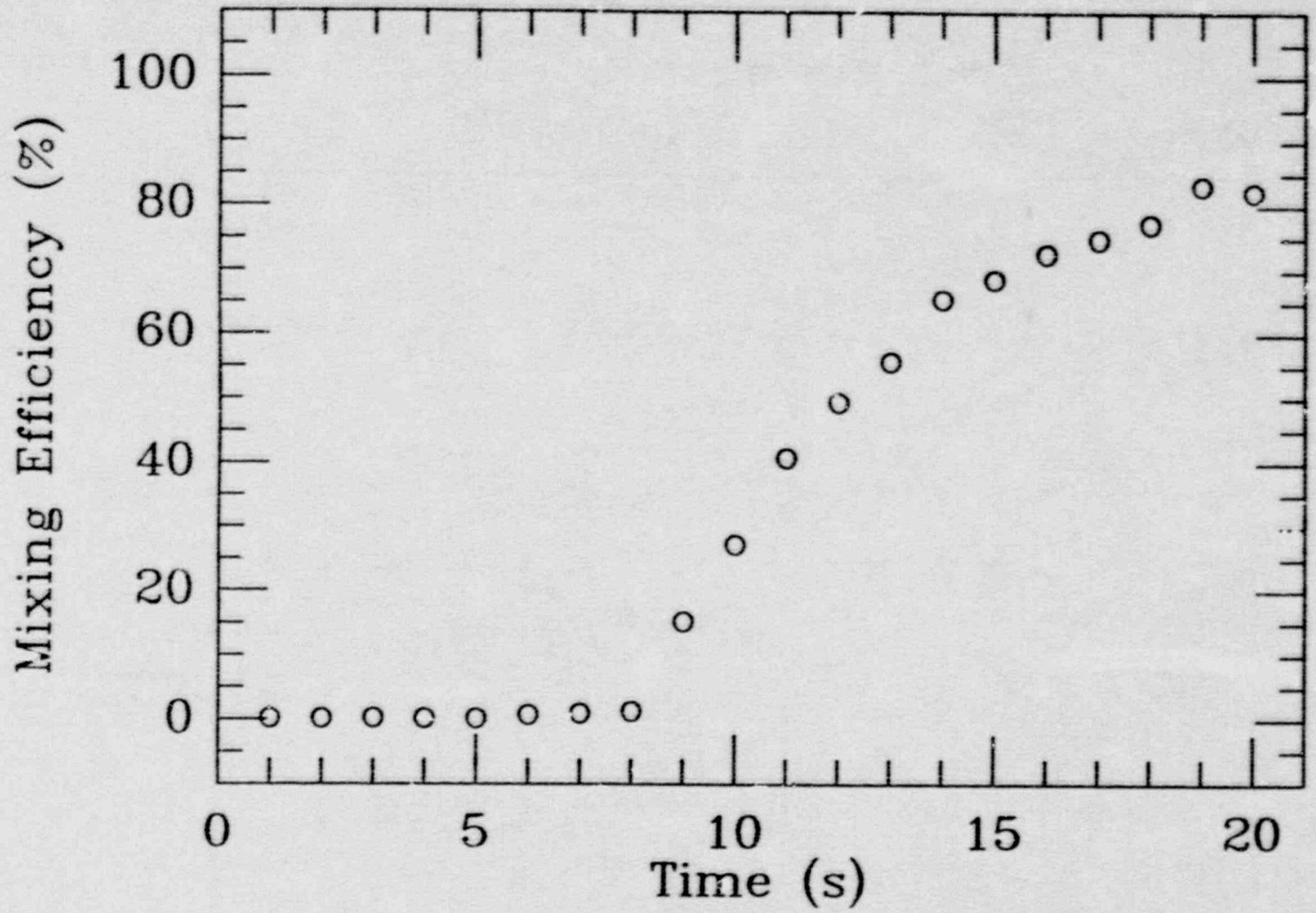

Fig. II-10b. *Mixing efficiency data (partial entrainment).*

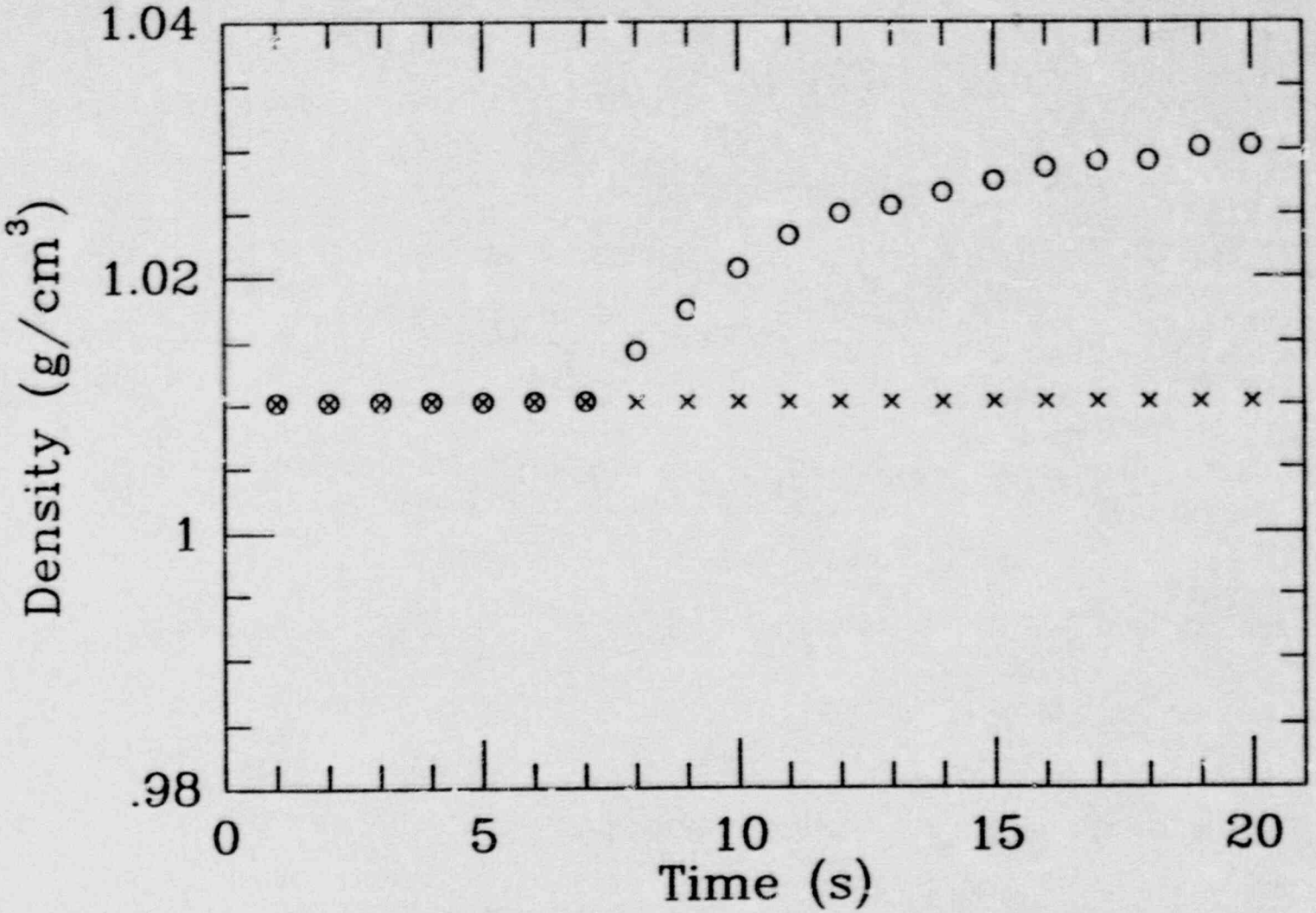

Fig. II-11a. *Inlet (x) and outlet (o) solute concentrations (partial entrainment).*

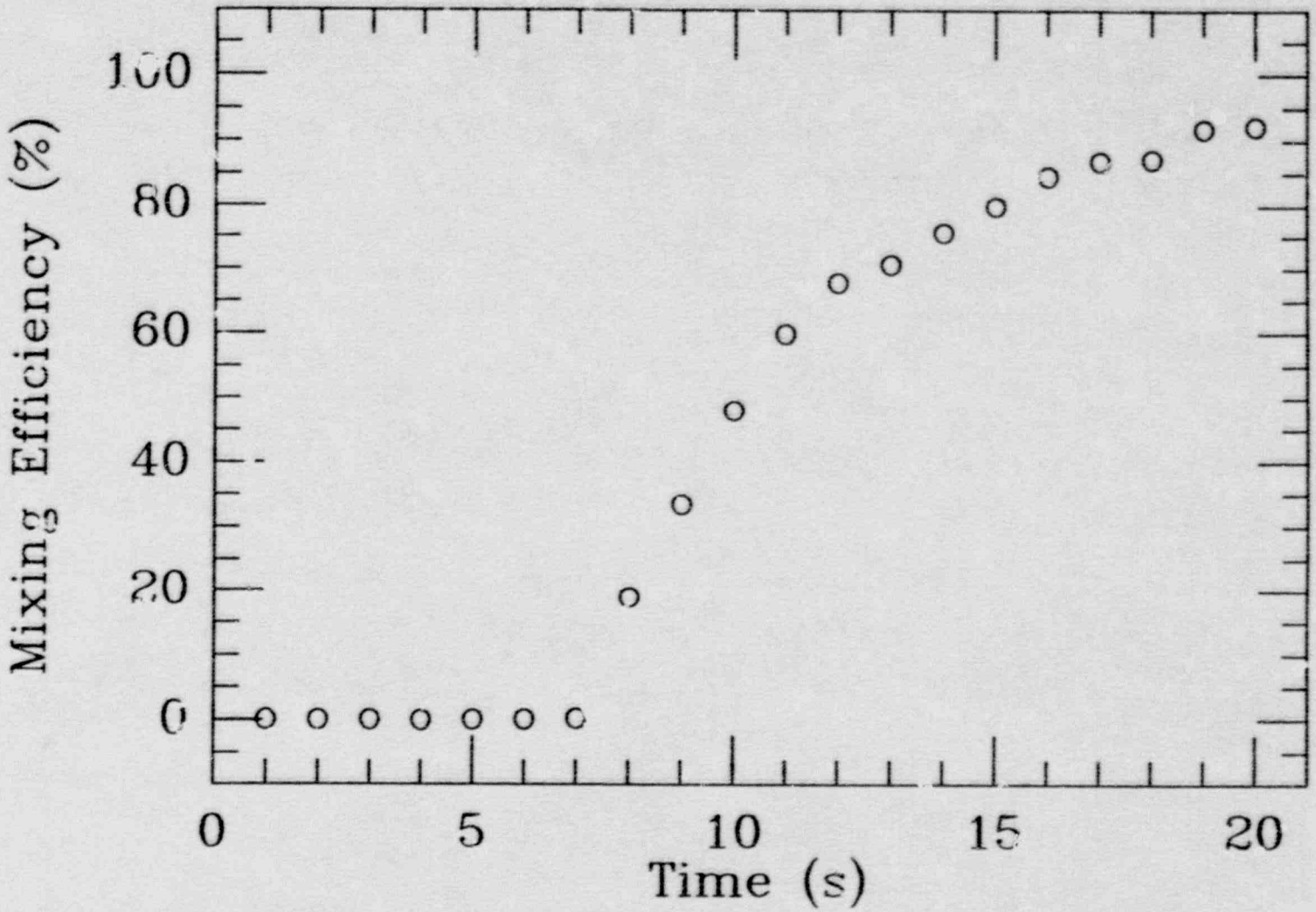

Fig. II-11b. *Mixing efficiency data (partial entrainment).*

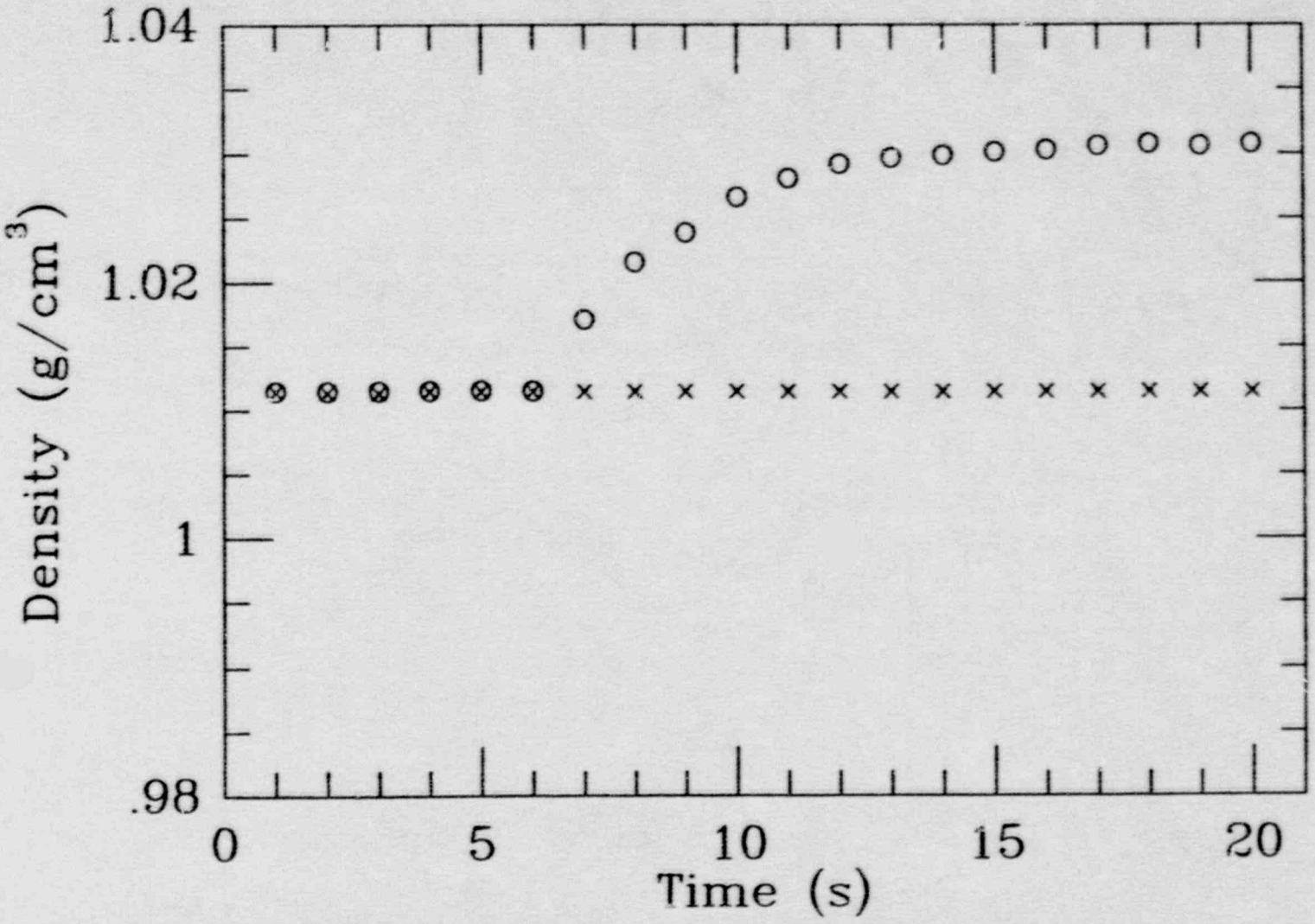

Fig. II-12a. *Inlet (x) and outlet (o) solute concentrations (partial entrainment).*

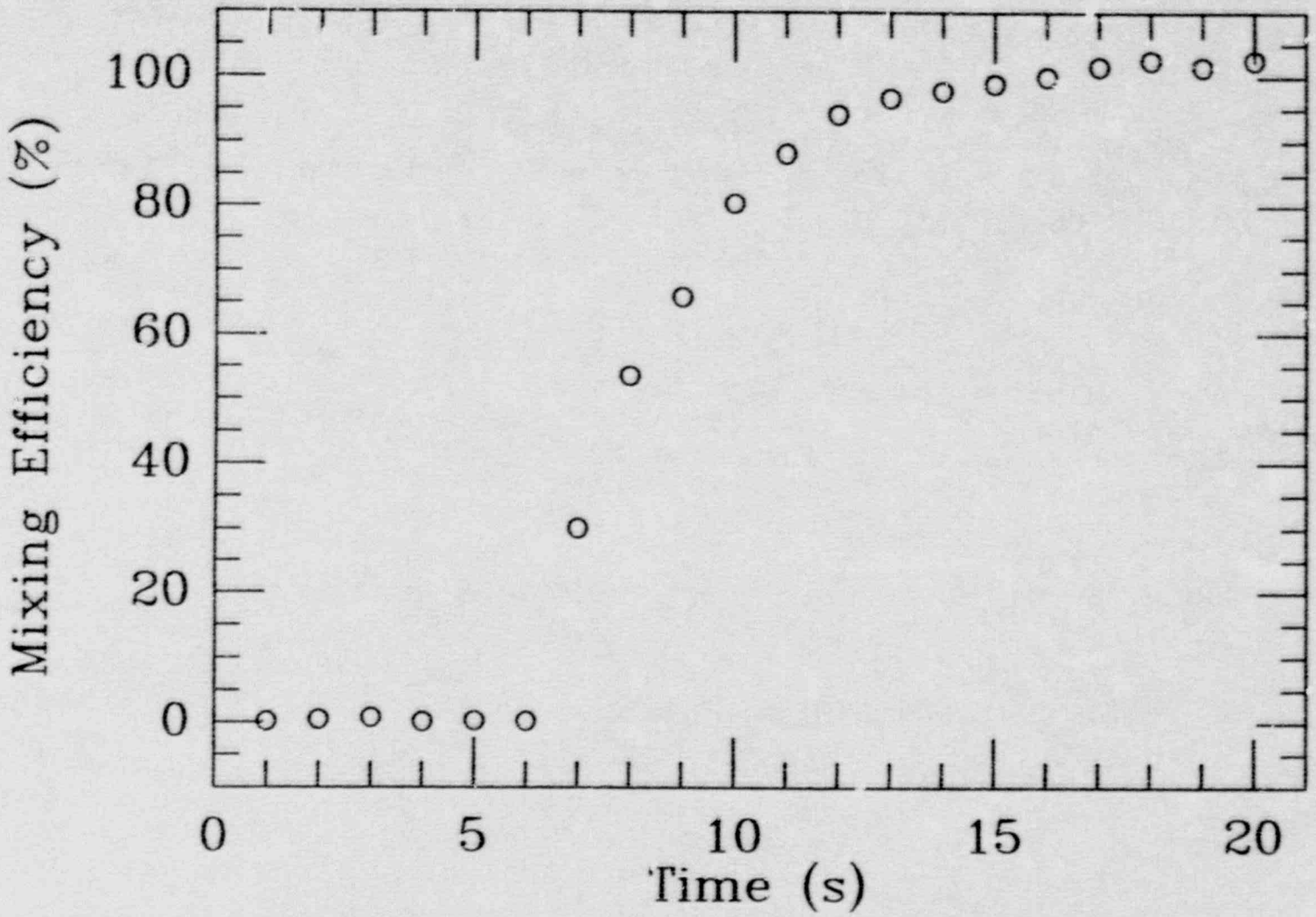

Fig. II-12b. *Mixing efficiency data (partial entrainment).*

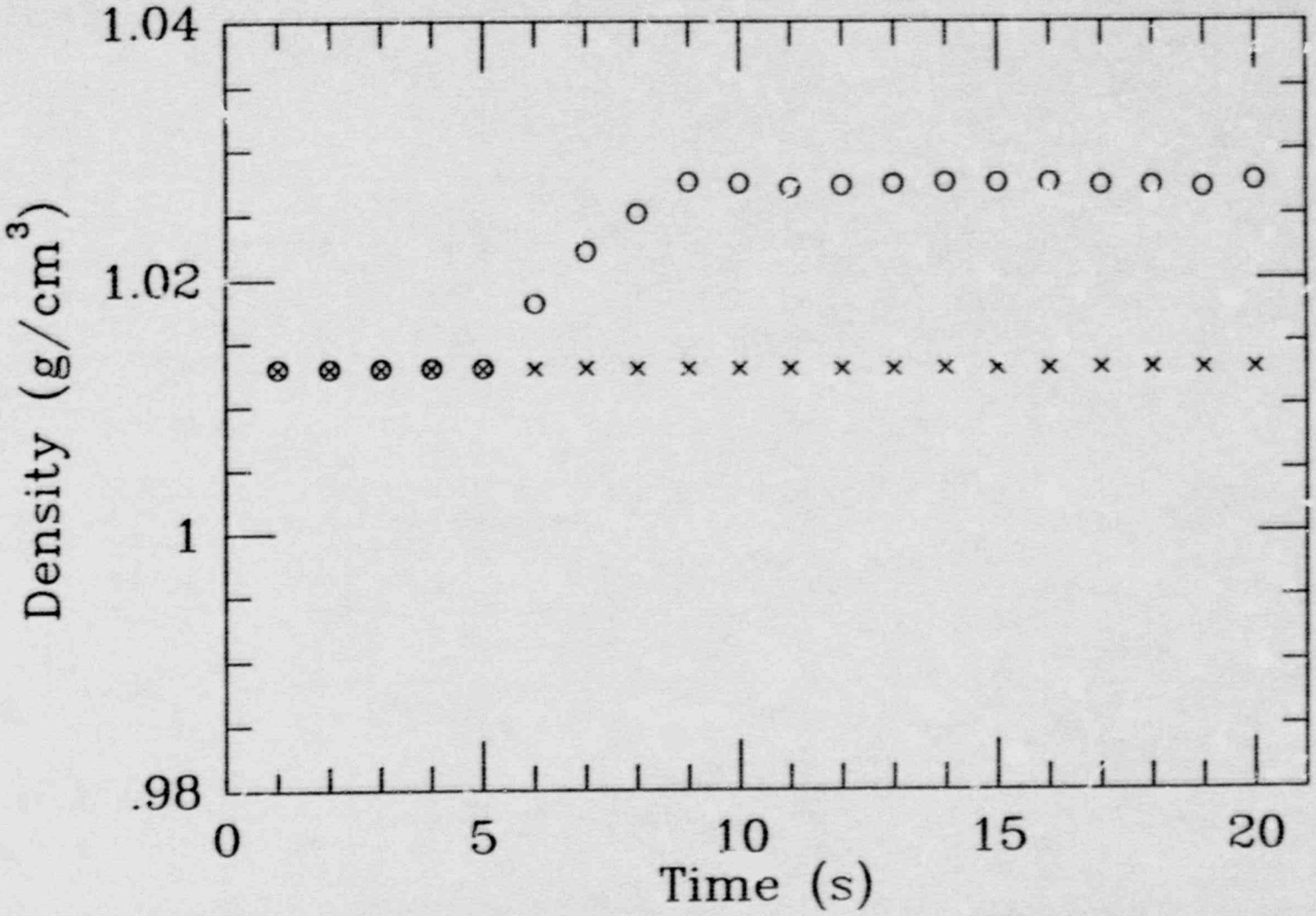

Fig. II-13a. *Inlet (x) and outlet (o) solute concentrations (full entrainment).*

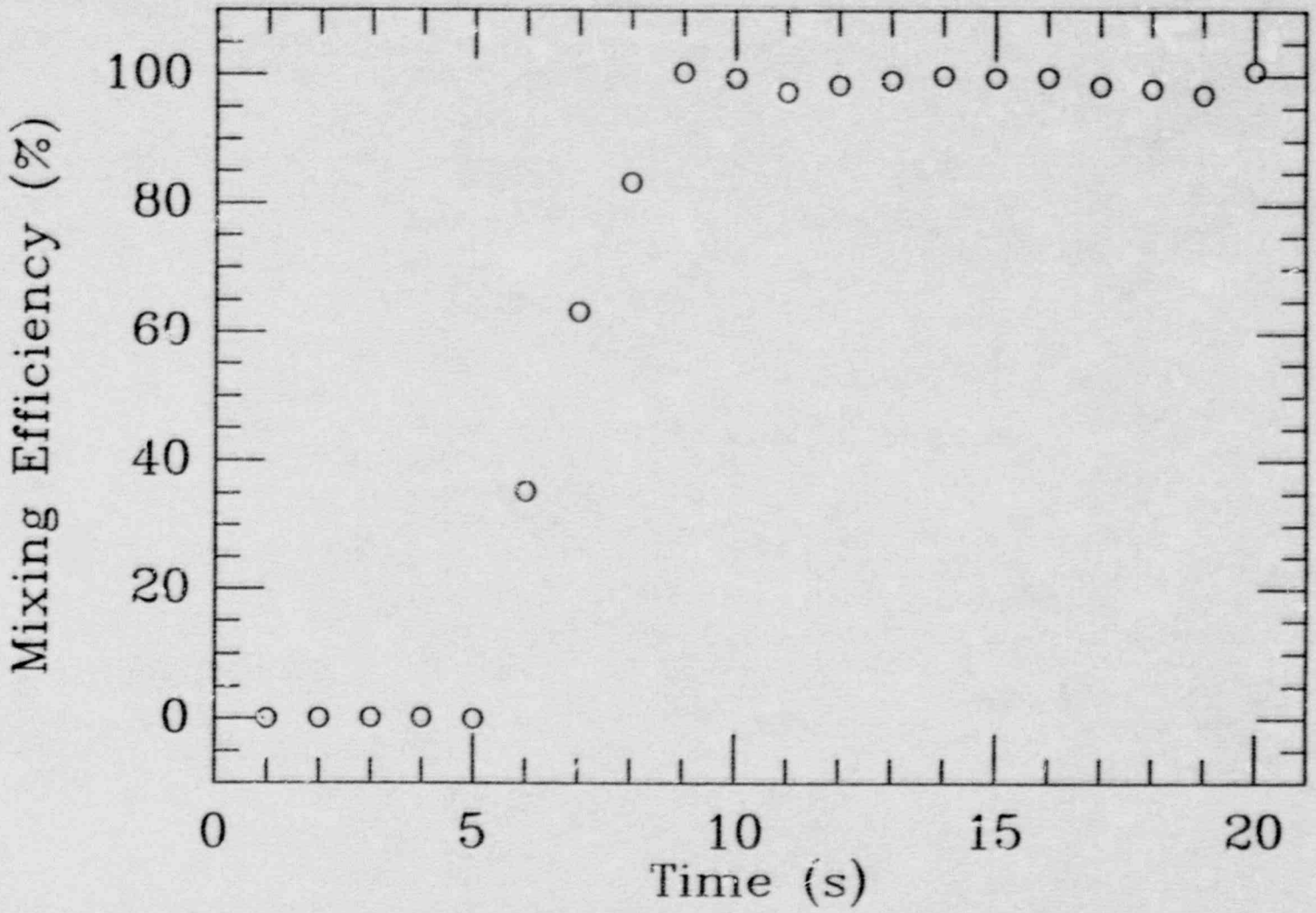

Fig. II-13b. *Mixing efficiency data (full entrainment).*

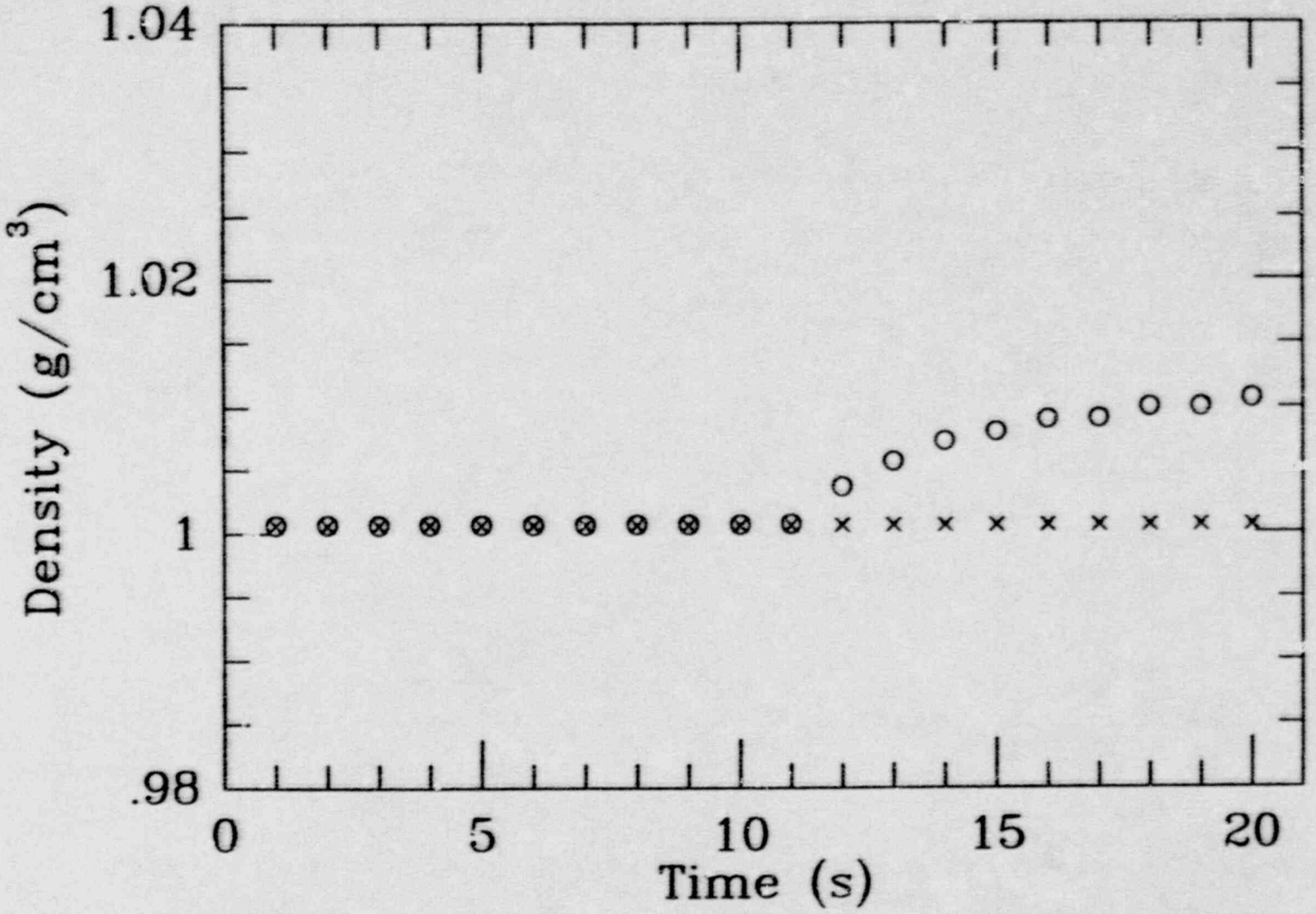

Fig. III-14a. *Inlet (x) and outlet (o) solute concentrations (partial entrainment).*

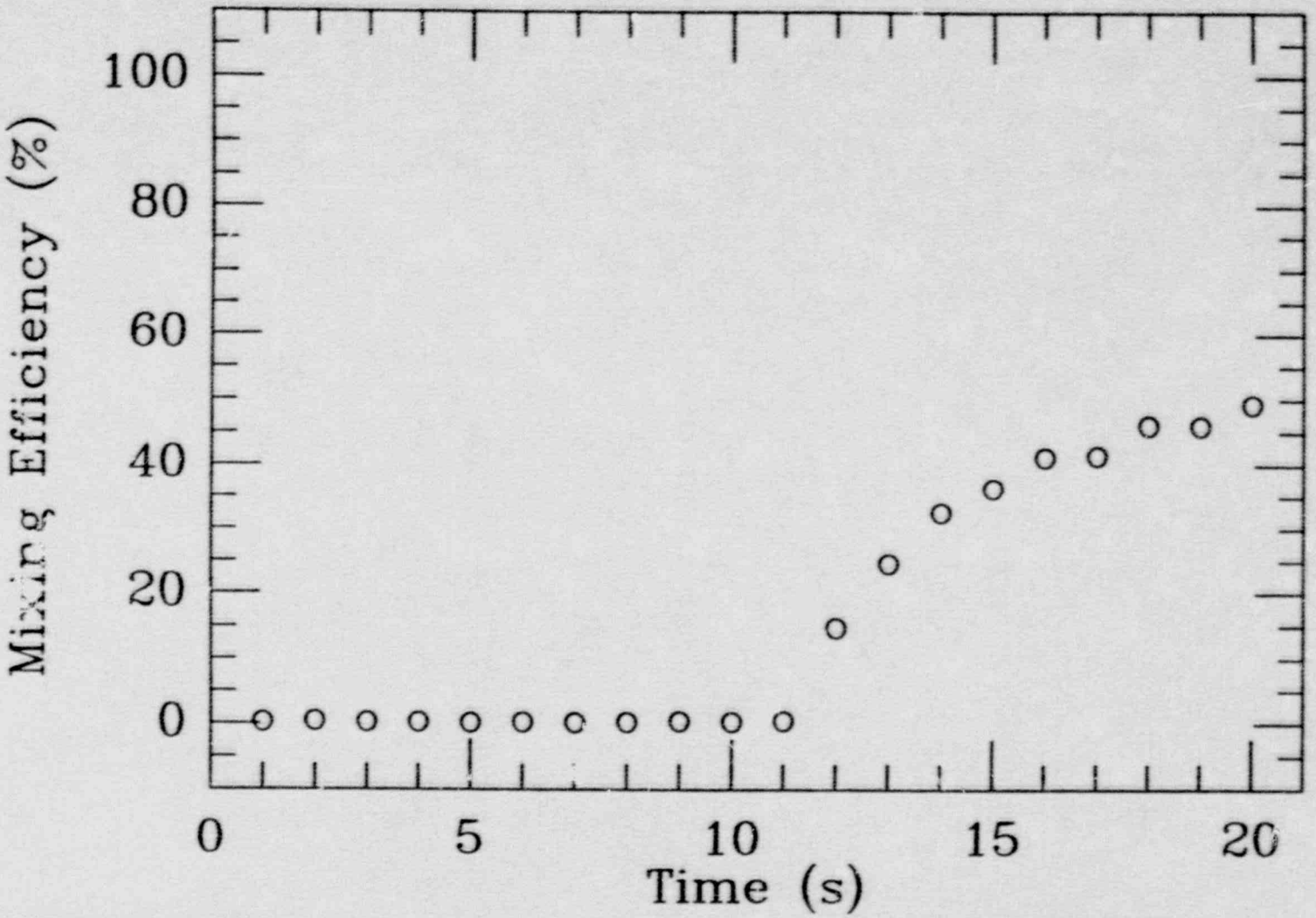

Fig. III-14b. *Mixing efficiency data (partial entrainment).*

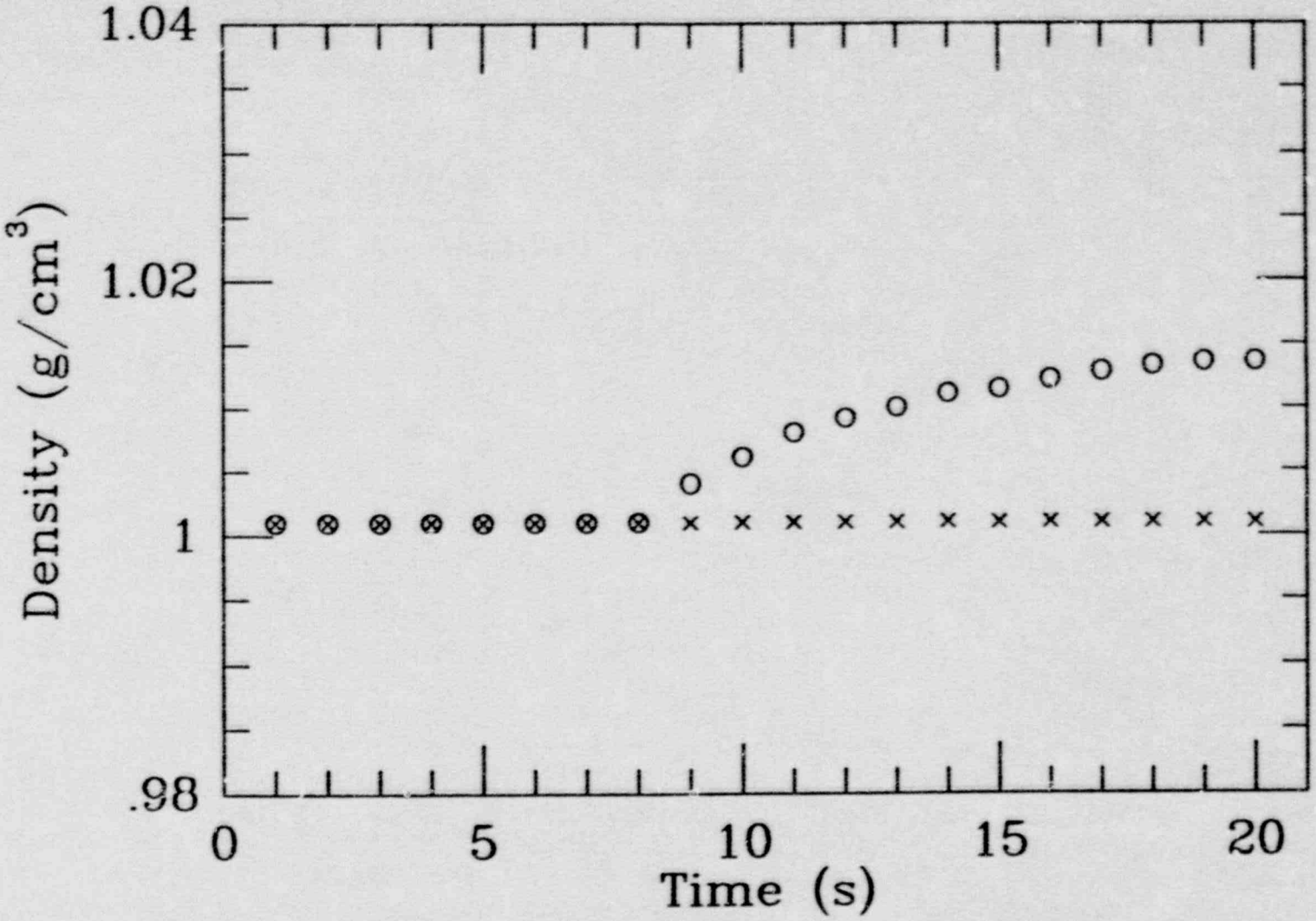

Fig. III-15a. *Inlet (x) and outlet (o) solute concentrations (partial entrainment).*

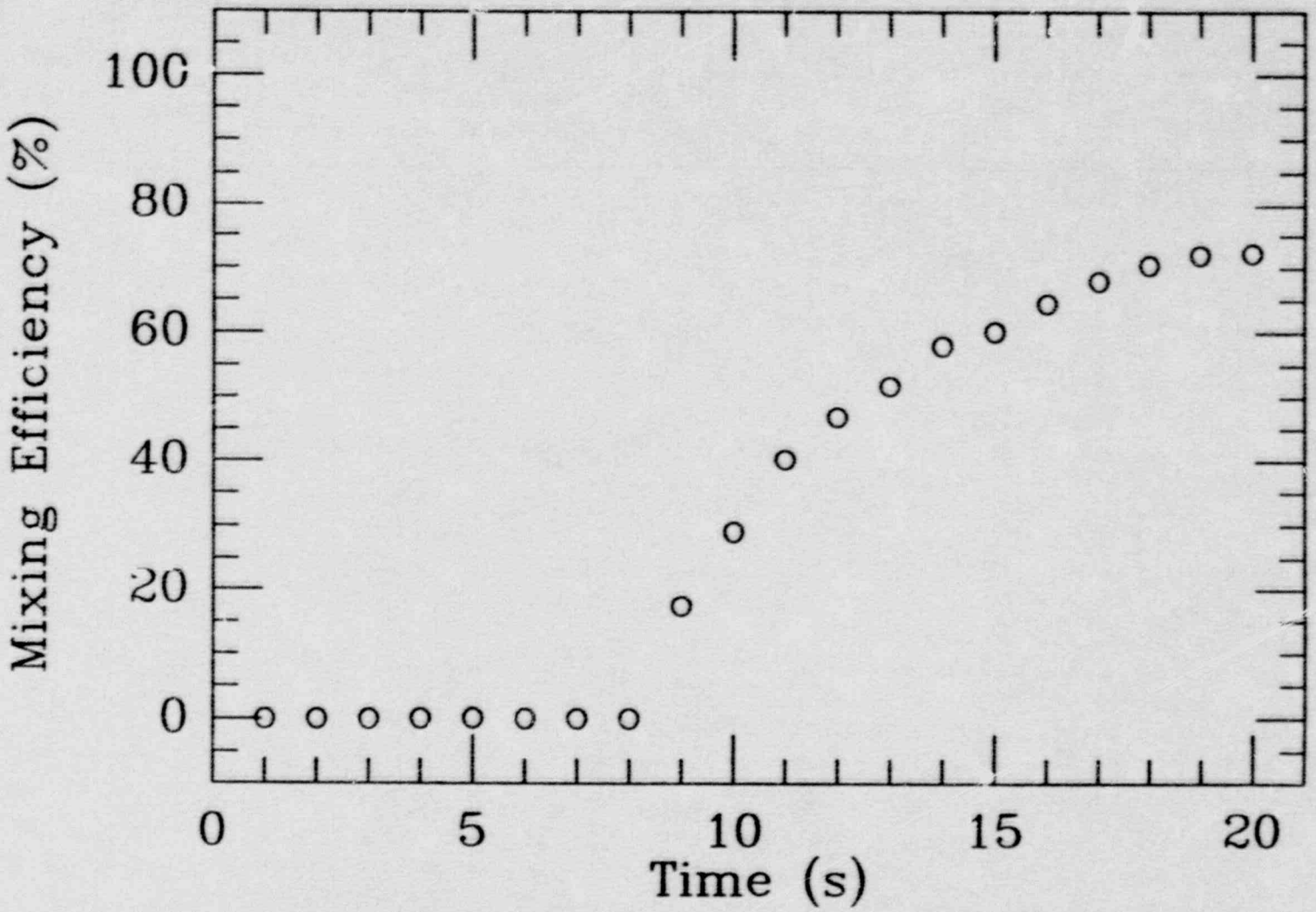

Fig. III-15b. *Mixing efficiency data (partial entrainment).*

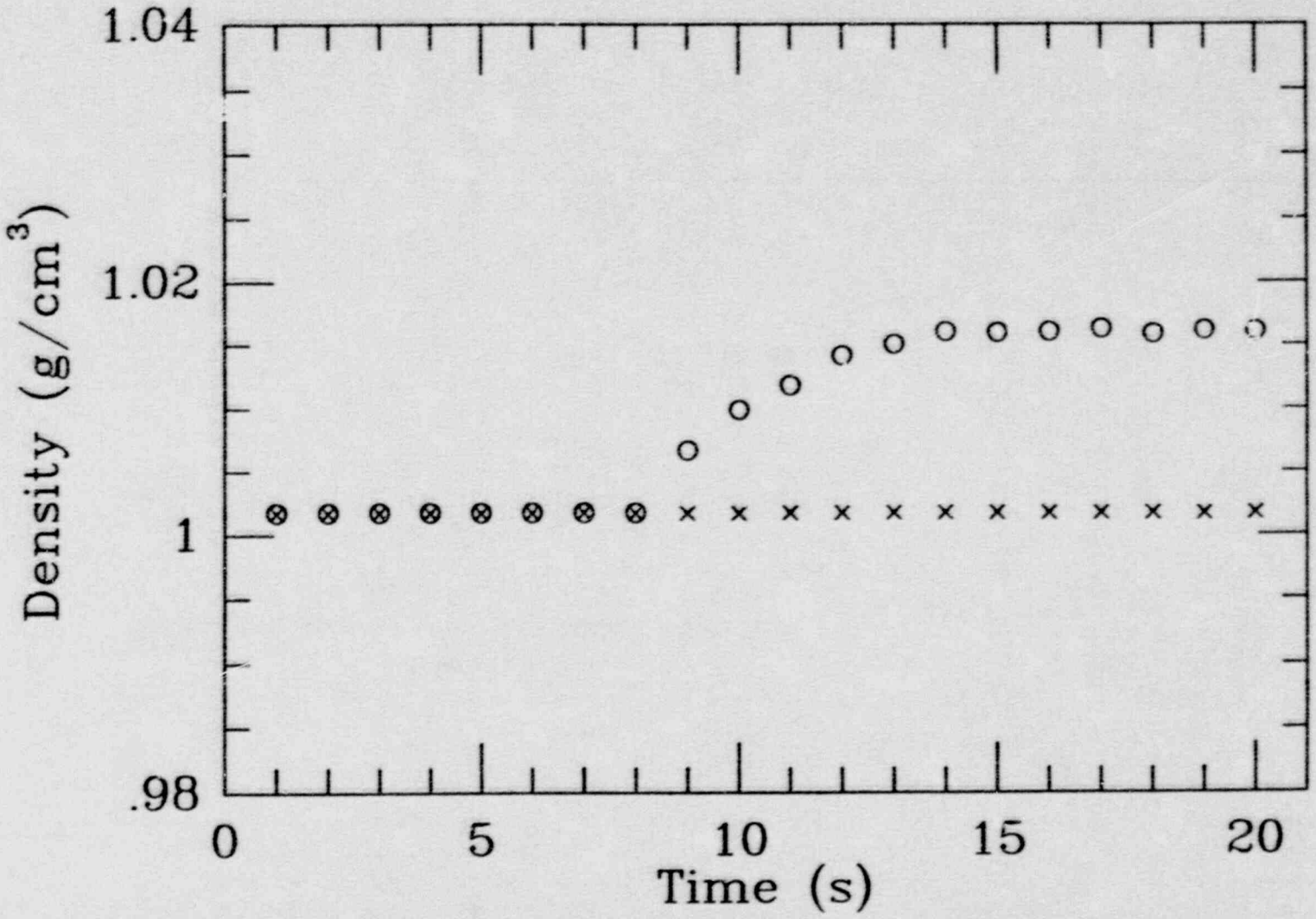

Fig. III-16a. *Inlet (x) and outlet (o) solute concentrations (full entrainment).*

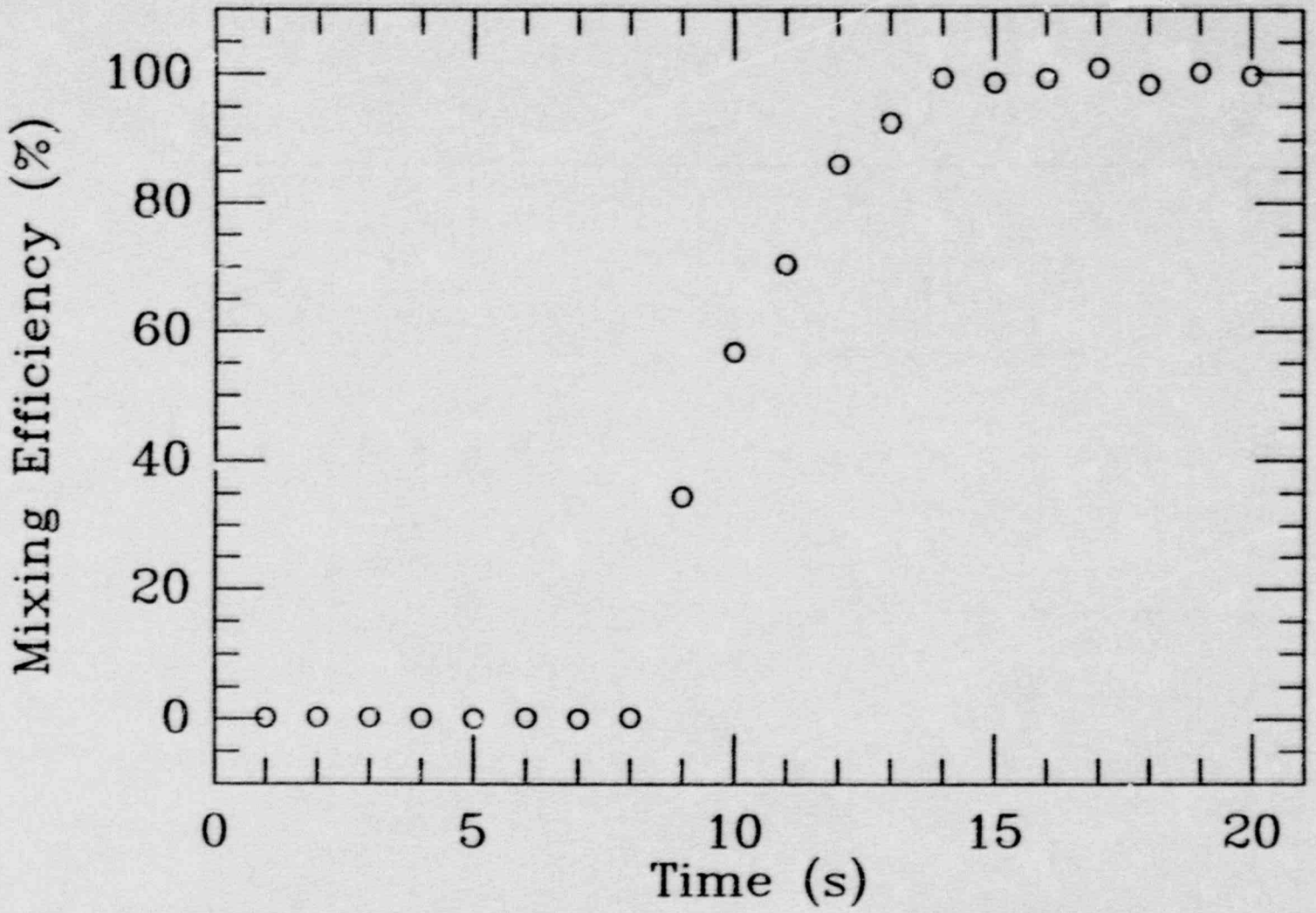

Fig. III-16b. *Mixing efficiency data (full entrainment).*

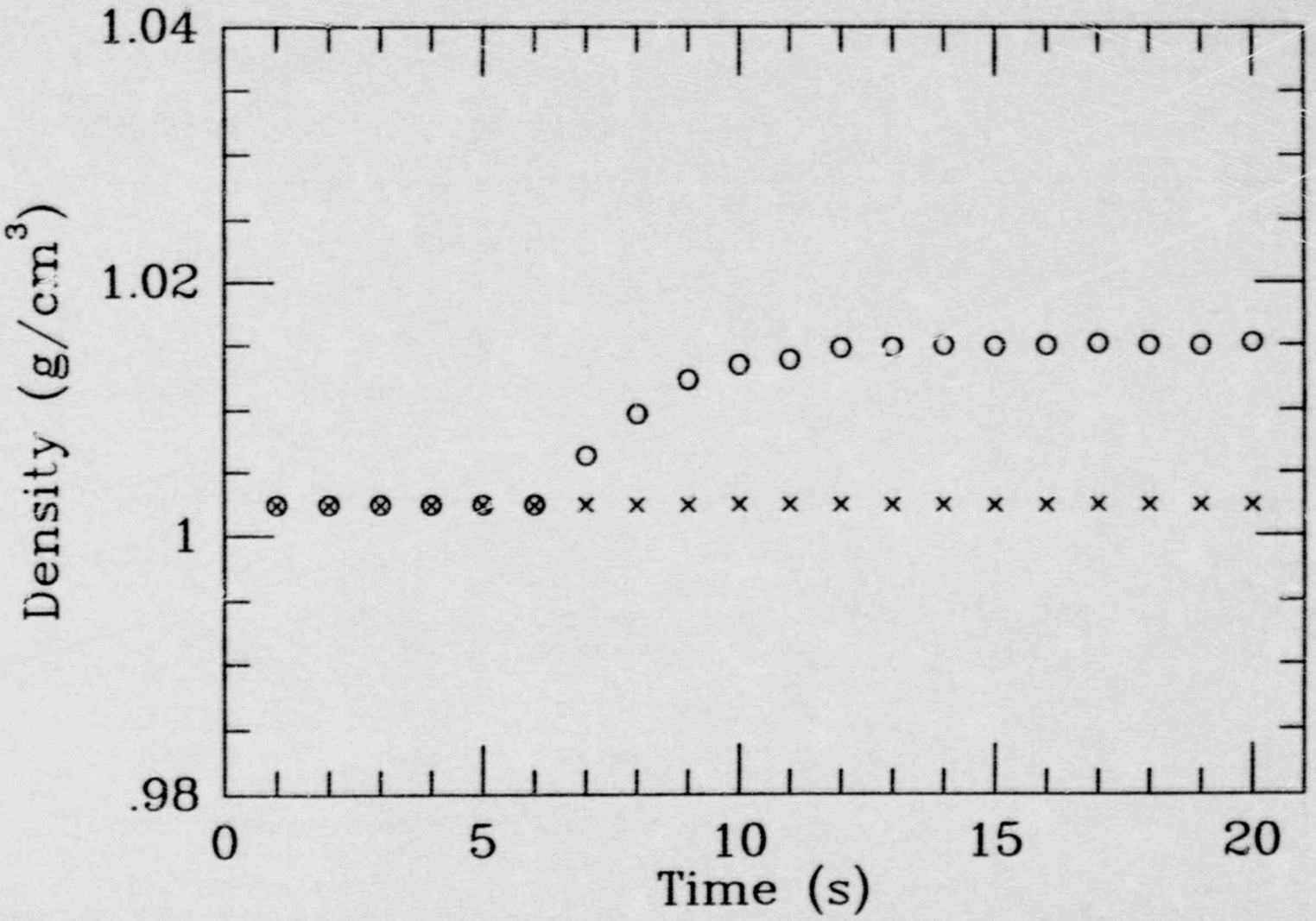

Fig. III-17a. *Inlet (x) and outlet (o) solute concentrations (full entrainment).*

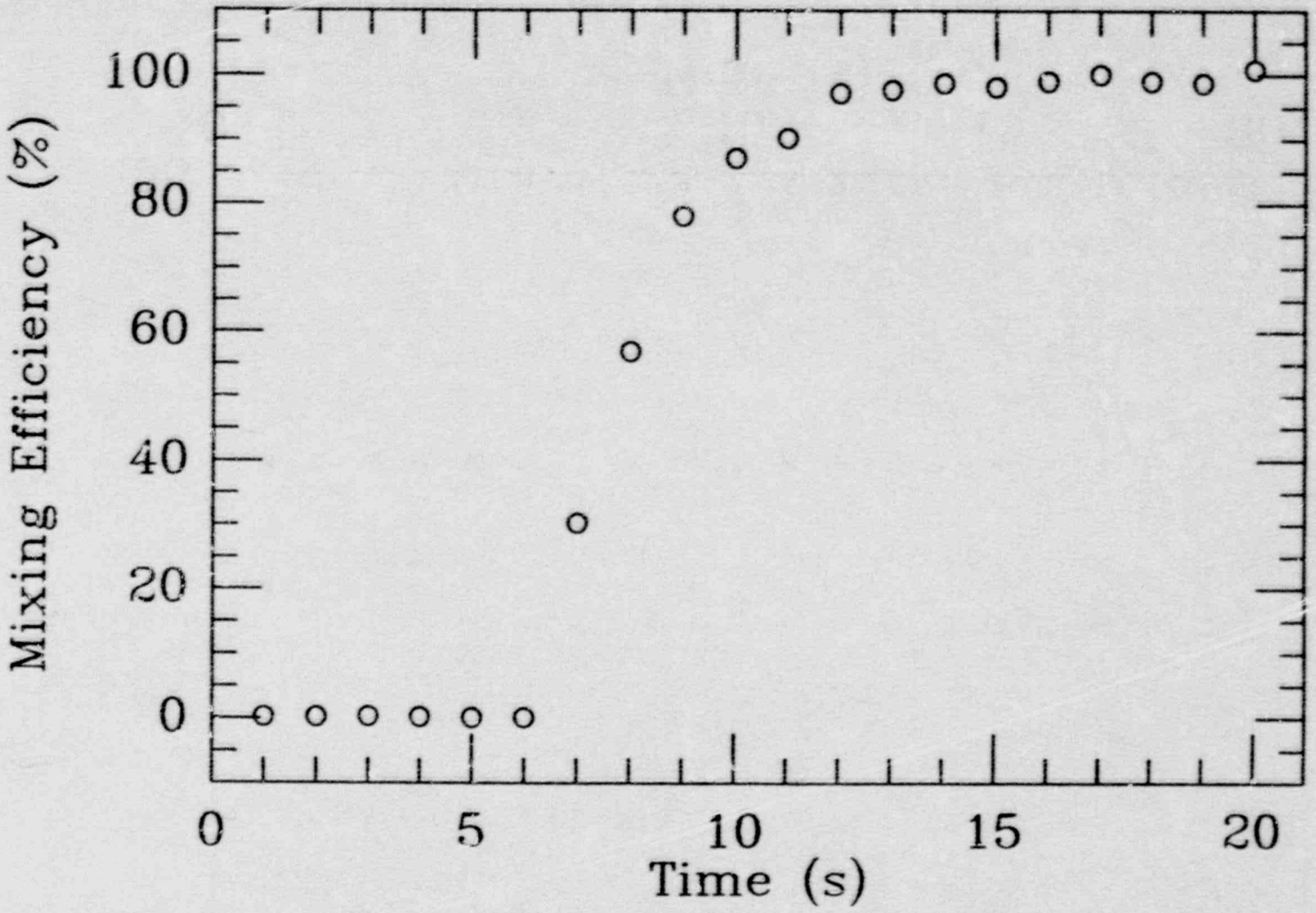

Fig. III-17b. *Mixing efficiency data (full entrainment).*

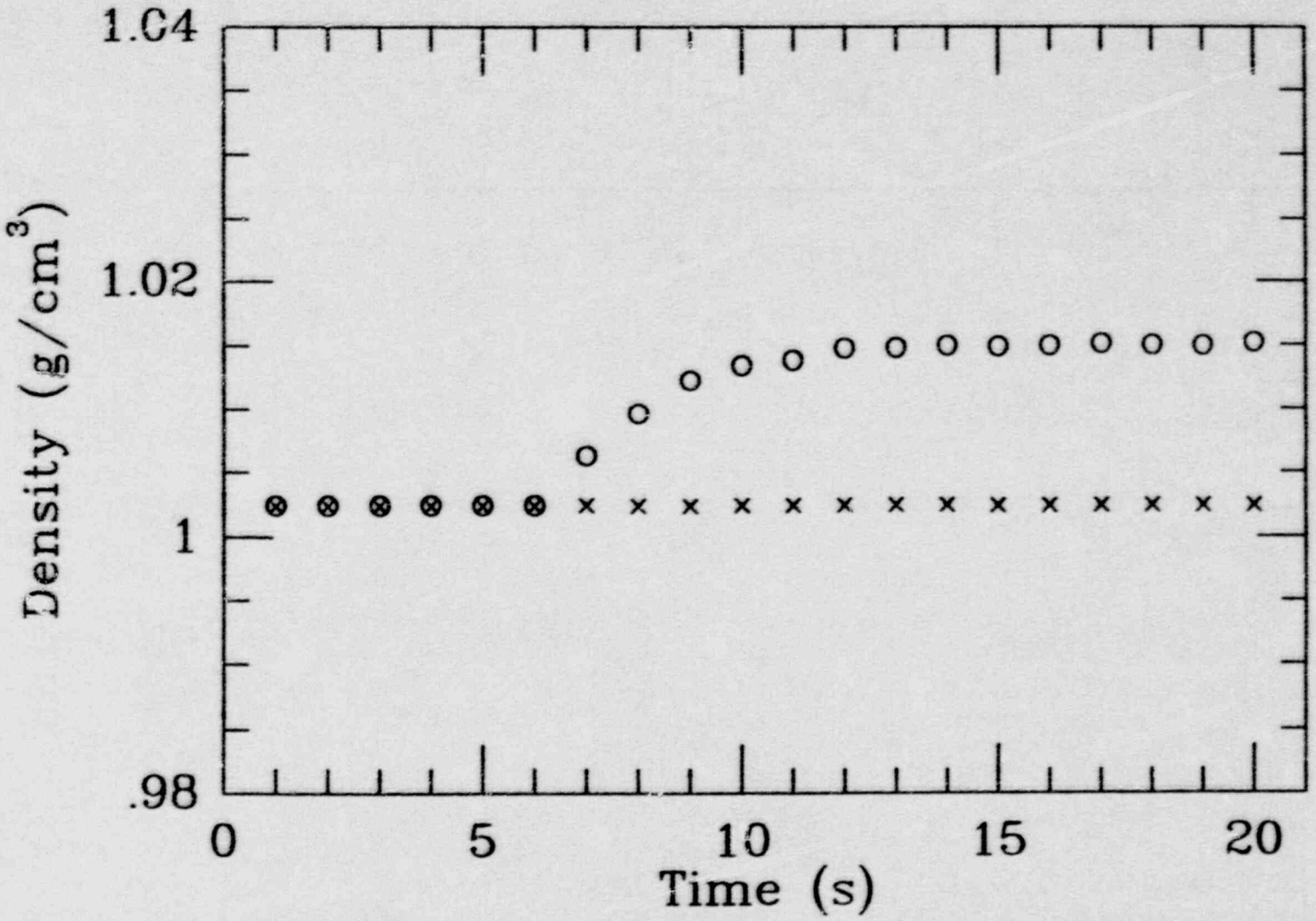

Fig. III-18a. *Inlet (x) and outlet (o) solute concentrations (full entrainment).*

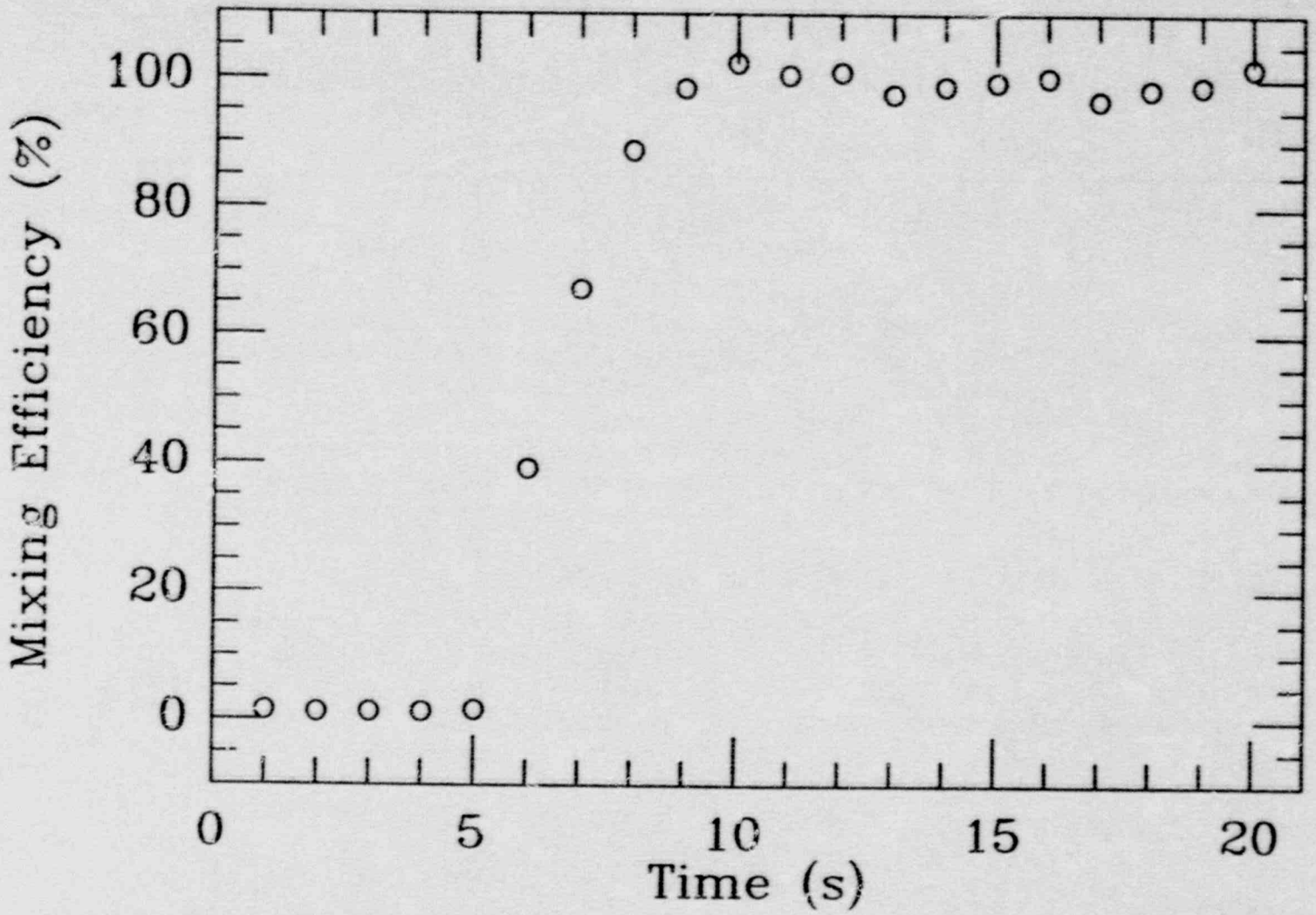

Fig. III-18b. *Mixing efficiency data (full entrainment).*

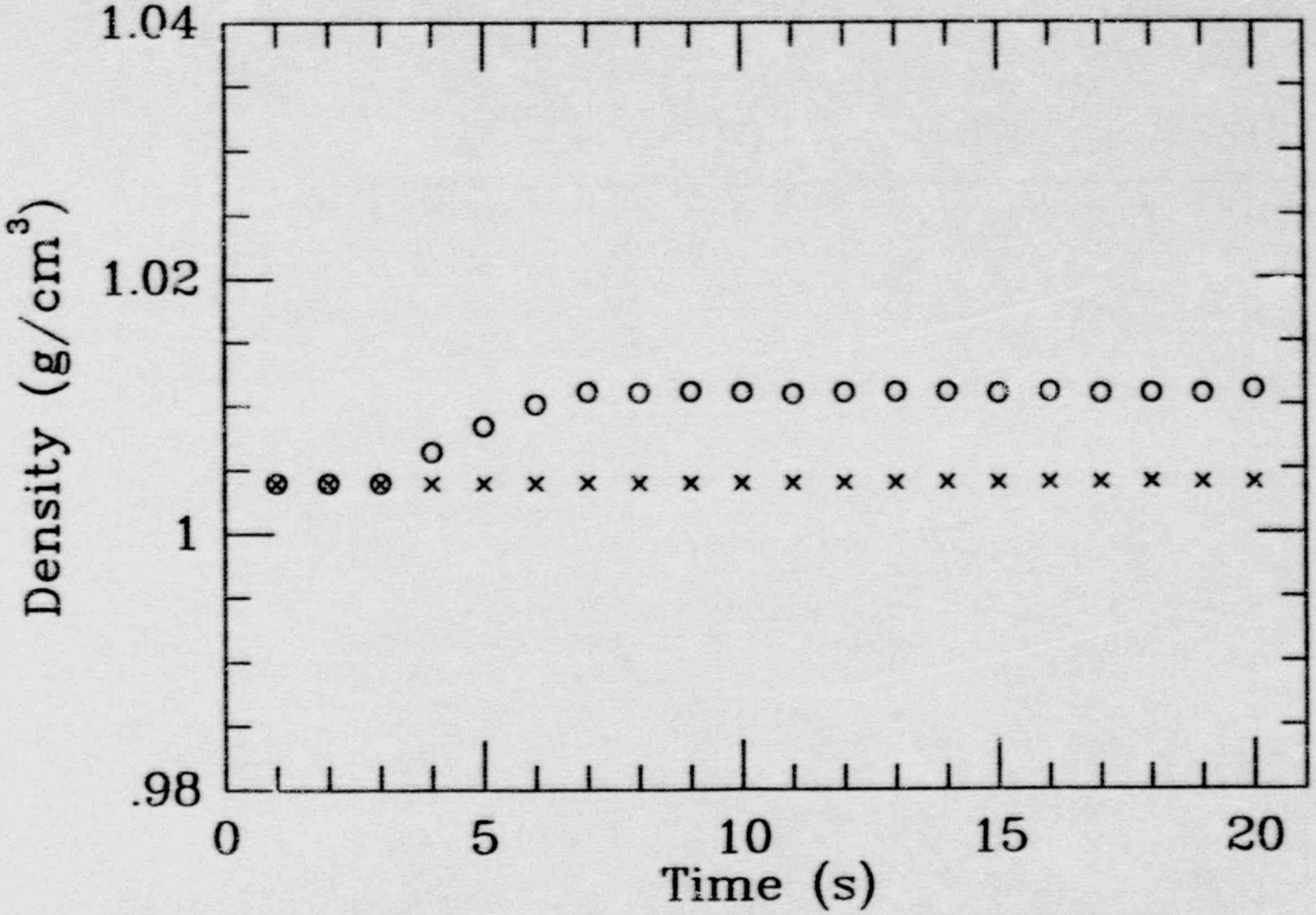

Fig. III-19a. *Inlet (x) and outlet (o) solute concentrations (full entrainment).*

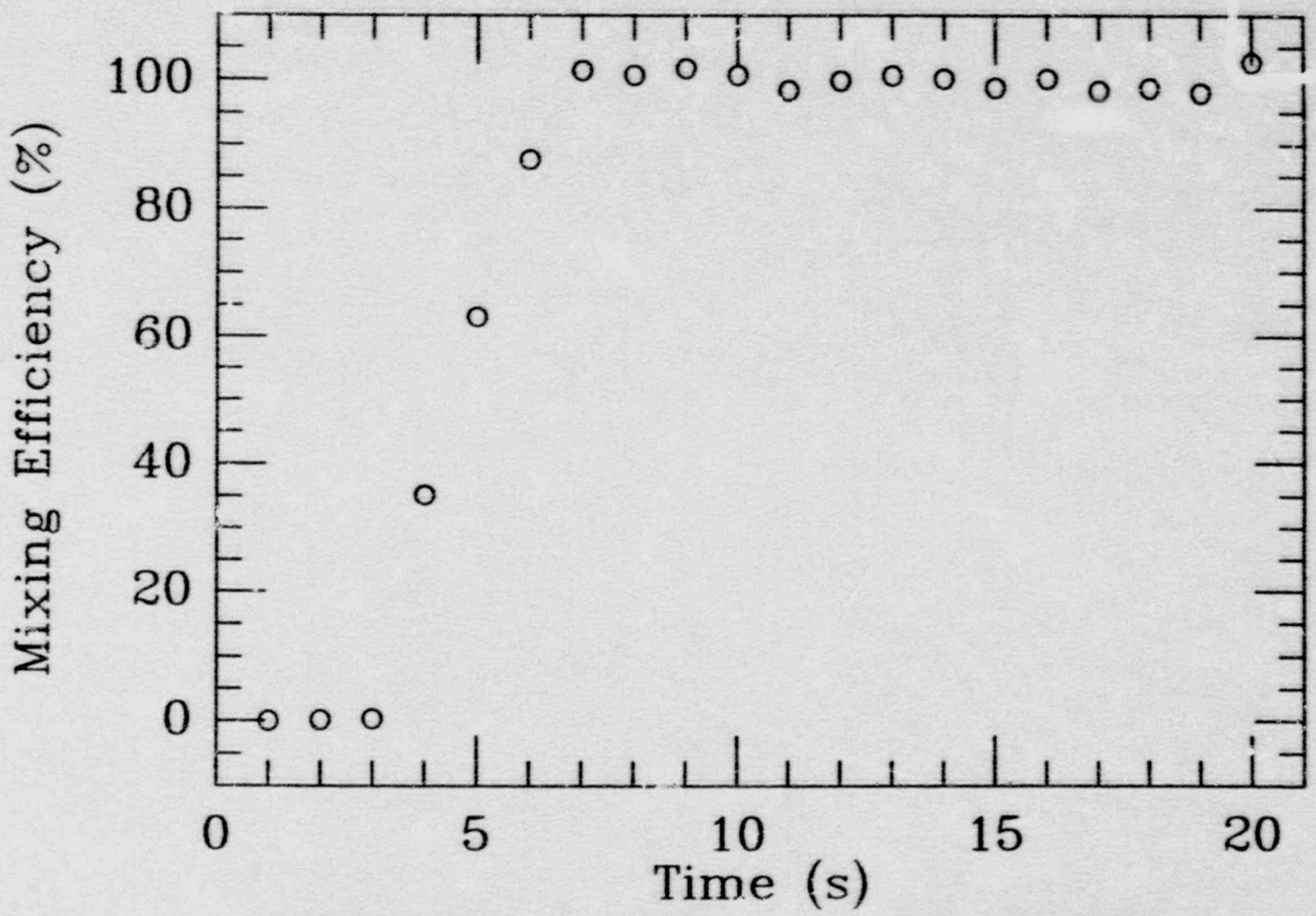

Fig. III-19b. *Mixing efficiency data (full entrainment).*

NRC FORM 335 (2-89) NRCM 1102, 3201, 3202

U.S. NUCLEAR REGULATORY COMMISSION

BIBLIOGRAPHIC DATA SHEET

(See instructions on the reverse)

1. REPORT NUMBER (Assigned by NRC, Add Vol., Supp., Rev., and Addendum Numbers, if any.)
NUREG/CR-5422

2. TITLE AND SUBTITLE
Performance of the Liquid Reactivity Control System in BWRs

3. DATE REPORT PUBLISHED
MONTH: September | YEAR: 1989

4. FIN OR GRANT NUMBER
D1634

5. AUTHOR(S)
T.G. Theofanous, E.A. Shabana

6. TYPE OF REPORT

7. PERIOD COVERED (Inclusive Dates)

8. PERFORMING ORGANIZATION – NAME AND ADDRESS (If NRC, provide Division, Office or Region, U.S. Nuclear Regulatory Commission, and mailing address; if contractor, provide name and mailing address.)
Department of Chemical and Nuclear Engineering
University of California
Santa Barbara, CA 93106

9. SPONSORING ORGANIZATION – NAME AND ADDRESS (If NRC, type "Same as above"; if contractor, provide NRC Division, Office or Region, U.S. Nuclear Regulatory Commission, and mailing address.)
Division of Regulatory Applications
Office of Nuclear Regulatory Research
U.S. Nuclear Regulatory Commission
Washington, DC 20555

10. SUPPLEMENTARY NOTES

11. ABSTRACT (200 words or less)

Boiling water reactors rely on the injection of soluble neutron absorbers to control power in case of failure in the control rod (scram) system. Typically this liquid "poison" is injected from eight small holes on a standpipe positioned vertically near the outer edge of the core shroud in the lower plenum. The achievement of control is predicated on good mixing of this injected liquid with the coolant which is recirculating around the core upper plenum and downcomer. However, because the flows are rather low (~20% of rated with pumps tripped as expected under such conditions) and the injected solution density is much higher than that of the primary fluid, there have been concerns raised about the efficiency and completeness of this mixing. This work provides the first openly available data addressing such concerns. To avoid potentially important scaling compromises, the data were obtained from full-scale simulations. From the experiments performed so far we can conclude that complete boron mixing (entrainment) will occur for recirculation flow rates down to 8.2% of rated.

12. KEY WORDS/DESCRIPTORS (List words or phrases that will assist researchers in locating the report.)
anticipated transients without scram (ATWS)
standby liquid control system (SLCS)
soluble neutron absorbers
boron mixing

13. AVAILABILITY STATEMENT
unlimited

14. SECURITY CLASSIFICATION
(This Page) unclassified
(This Report) unclassified

15. NUMBER OF PAGES

16. PRICE

NRC FORM 335 (2-89)

UNITED STATES
NUCLEAR REGULATORY COMMISSION
WASHINGTON, D.C. 20555